DAAG MARSHALL

THE INVESTIGATION OF TETHERED SATELLITE SYSTEM DYNAMICS

Contract NAS8-36160

Quarterly Report #3

For the period 15 February 1985 through 14 May 1985

Principal Investigator
Dr. Enrico Lorenzini

June 1985

Prepared for
National Aeronautics and Space Administration
Marshall Space Flight Center, Alabama 35812

Smithsonian Institution
Astrophysical Observatory
Cambridge, Massachusetts 02138

The Smithsonian Astrophysical Observatory
is a member of the
Harvard-Smithsonian Center for Astrophysics

THE INVESTIGATION OF TETHERED SATELLITE SYSTEM DYNAMICS

Contract NAS8-36160

Quarterly Report #3

For the period 15 February 1985 through 14 May 1985

Principal Investigator
Dr. Enrico Lorenzini

Co-Investigators
Mr. David A. Arnold
Dr. Mario D. Grossi
Dr. Gordon E. Gullahorn
Mr. William Harrold
Prof. Robert G. Hohlfeld

June 1985

Prepared for
National Aeronautics and Space Administration
Marshall Space Flight Center, Alabama 35812

Smithsonian Institution
Astrophysical Observatory
Cambridge, Massachusetts 02138

CONTENTS

CONTENTS (Cont.)

Abstract

The content of this Quarterly Report can be summarized as follows:

a) The tether control law to retrieve the satellite has been modified in order to have a smooth retrieval trajectory of the satellite that minimizes the thruster activation.

b) The satellite thrusters have been added to our rotational dynamics computer code and a preliminary control logic has been implemented to simulate them during the retrieval maneuver.

c) The high resolution computer code for modelling the three-dimensional dynamics of untensioned tether, SLACK3, has been made fully operative and a set of computer simulations of possible tether breakages has been run.

d) The distribution of the electric field around an electrodynamic tether in vacuo severed at some length from the Shuttle has been computed with a three-dimensional electrodynamic computer code.

1.0 INTRODUCTION

This is the third quarterly report submitted by SAO under contract NAS8-36160, "The Investigation of Tethered Satellite System Dynamics," Dr. Enrico Lorenzini, PI, and covers the period from 15 February 1985 through 14 May 1985.

2.0 TECHNICAL ACTIVITY DURING REPORTING PERIOD AND PROGRAM STATUS

2.1 Retrieval Control Law

The existing version of the DUMBEL program including the rotation of the subsatellite does not have a retrieval control law, but is easily modified to include various control laws. For this project a modified version of the control law used in program TETHER has been incorporated into DUMBEL. The TETHER program developed at Marshall Space Flight Center uses a tension control law of the form:

$$T = m_e(\omega_c^2(\ell - \ell_c) + 3\omega_o^2(\ell + \text{BOOM}) + 2\xi_c\omega_c(\dot{\ell} - \dot{\ell}_c)) \qquad (2.1.1)$$

where

T = tether tension
m_e = effective mass ($m_{SAT} + m_{TETH}/2$)
ξ_c = control law damping
ω_o = orbital frequency
BOOM = boom length
ℓ = tether length

$$\ell_c = \ell_o e^{-.00035t_c} + \text{BOOM} \qquad (2.1.2)$$
$$\dot{\ell}_c = -.00035\ell_c$$

neglecting the effect of the boom, the control frequency is

$$\omega_c = 2\omega_o \qquad (2.1.3)$$

The time t_c is the time measured from the start of retrieval. The first term keeps the retrieval on a specified time schedule, the second provides the equilibrium tension required to support the subsatellite, and the third provides damping and controls the rate of retrieval. The control law is used in conjunction with thrusters to allow rapid retrieval. The law may be used with arbitrary initial conditions. For a 20 km tether, the initial commanded retrieval rate is 700 cm/sec.

2.1.1 Retrieval At A Constant In-Plane Deflection Angle -

The equation of motion for the in-plane deflection, if we neglect the tether mass, is

$$F_\theta = m_2(\ddot{\theta}\ell\cos\phi + 2(\dot{\theta}+\omega_o)(\dot{\ell}\cos\phi - \ell\dot{\phi}\sin\phi) + 3\ell\omega_o^2\cos\theta\cos\phi\sin\theta) \qquad (2.1.4)$$

Where m_2 is the satellite mass. If we have $\phi = \dot{\phi} = \dot{\theta} = F_\theta = 0$, then the equation of motion reduces to

$$0 = m_2(2\omega_o\dot{\ell} + 3\ell\omega_o^2\cos\theta\sin\theta)$$

Solving for the retrieval rate we have

$$\dot{\ell} = -\frac{3}{2}\ell\omega_o\cos\theta\sin\theta \qquad (2.1.5)$$

$$\dot{\ell} = -\alpha\ell \qquad (2.1.6)$$

where

$$\alpha = \frac{3}{2}\omega_o\cos\theta\sin\theta \qquad (2.1.7)$$

The distance ℓ as a function of time is, by integration

$$\ell = \ell_0 e^{-\alpha t} \tag{2.1.8}$$

The acceleration is

$$\ddot{\ell} = -\alpha\dot{\ell} = \alpha^2\ell \tag{2.1.9}$$

The equation of motion of the radial variable is

$$\tau = m_2(\ddot{\ell} - \ell\dot{\phi}^2 - \ell\cos^2\phi\,(\dot{\theta} + \omega_0)^2 + \ell\omega^2_0 - 3\ell\omega_0^2\cos^2\theta\cos^2\phi) \tag{2.1.10}$$

If we have $\phi = \dot{\phi} = \dot{\theta} = 0$, the equation reduces to

$$\tau = m_2(\ddot{\ell} - 3\ell\omega_0^2\cos^2\theta) \tag{2.1.11}$$

In order to implement a tension control law we need to evaluate $\ddot{\ell}$ in order to calculate the tension τ. For retrieval at a constant angle θ, the acceleration is, from equations (2.1.9) and (2.1.7)

$$\ddot{\ell} = \alpha^2\ell = \frac{9}{4}\omega_0^2\cos^2\theta\sin^2\theta\,\ell \tag{2.1.12}$$

Putting equation (2.1.12) into equation (2.1.11) gives

$$\tau = m_2(\frac{9}{4}\omega_0^2\cos^2\theta\sin^2\theta\,\ell - 3\ell\omega_0^2\cos^2\theta) = 3m_2\ell\omega_0^2\cos^2\theta\,(\frac{3}{4}\sin^2\theta - 1) \tag{2.1.13}$$

In the equation for the tension, the distance ℓ should be measured from the orbital center of the system. For a system of masses m_1 = Shuttle and m_2 = satellite, the distance of m_2 from the center of mass of the system is $\ell m_1/(m_1 + m_2)$.

For a simple harmonic oscillator of frequency ω, the critical damping coefficient is

$$b = 2m\omega \tag{2.1.14}$$

For the in-plane variable θ, the frequency is $\sqrt{3}\omega_0$. For the out-of-plane

variable ϕ the frequency is $2\omega_o$ and the critical damping coefficient is $4m\omega_o$.

In equation (2.1.4) we see from the last term that the restoring term is approximately $3m\ell\omega_o^2\theta$ for small angles. The stiffness is therefore $3m\omega_o^2$, since $\ell\theta$ is the in-plane displacement. For the out-of-plane variable the stiffness obtained for small displacements is $4m\omega_o^2$.

In the control law of equation (2.1.1) the first term is designed to keep the motion along the trajectory prescribed by the commanded length. The stiffness is the same as the out-of-plane restoring stiffness. The last term is designed to provide damping and uses the coefficient for critical damping of out-of-plane oscillations. The middle term is designed to provide the equilibrium tension necessary to balance the gravity gradient.

The retrieval profile given in equation (2.1.2) will produce an in-plane displacement which can be calculated from equation (2.1.7). With ω_o = .00113137, the retrieval angle for α = .00035 is 12.18 degrees. The initial retrieval rate for a 20 km tether is $\alpha\ell_o$ = 7 m/sec.

The first term in equation (2.1.1) is not necessary for maintaining the stability of the retrieval. As an alternative to forcing the retrieval to "catch up" to a desired time table, one could omit the first term and allow the retrieval to proceed in a natural way and determine the time required for retrieval from a hanging position. The difference between this time and the time calculated from the commanded length can be used as a correction factor to adjust the start time of the retrieval to obtain a desired termination time. The first term can have the effect of forcing the retrieval in a way that may not have a beneficial effect on stability. The value of ℓ_c in the last term does not necessarily have to be computed from ℓ_c. It could be computed as

$$\dot{\ell}_c = -\alpha\ell \qquad (2.1.15)$$

This should promote stability by bringing the retrieval rate to the value necessary for maintaining the desired retrieval angle for the actual length of the wire at any particular time. If the retrieval is on a perfect trajectory the first and third terms will be zero since $\ell = \ell_c$ and $\dot{\ell} = \dot{\ell}_c$. The second term should then provide the tension necessary to maintain a perfect retrieval trajectory. The second term in equation (2.1.1) is obtained by setting $\ddot{\ell} = \theta = 0$ in equation (2.1.11). A more accurate expression can be obtained by taking into account the deceleration, the dependence of the tension on the in-plane angle, and the correction for the location of the center of mass of the system. The center of mass is not exactly the same as the point of zero radial acceleration but the difference can be neglected for this purpose. An alternative control law taking into account the above considerations is

$$T = 3m_e\ell\omega_o^2\cos^2\theta_c\left(\frac{3}{4}\sin^2\theta_c - 1\right)m_1/(m_1+m_2) + 4\omega_o(\dot{\ell} - \dot{\ell}_c) \qquad (2.1.16)$$

where

$$\dot{\ell}_c = -\alpha\ell$$

$$\alpha = \frac{3}{2}\omega_o\cos\theta_c\sin\theta_c = \frac{3}{4}\omega_o\sin(2\theta_c)$$

In equation (2.1.16) the angle θ_c is a fixed parameter of the tether control law. The value of θ_c determines the duration of the maneuver. It also represents the inclination of the steady state trajectory followed by the satellite during retrieval.

2.1.2 Software Modifications -

There are two versions of DUMBEL. One has rotation of the subsatellite and the other does not. The version with rotation does not have many of the special features included in the other version. In order to have an initial in-plane displacement in the rotational version it was necessary to add some subroutines from the other version. This turned out to be more difficult than anticipated because the numbering of the masses in the rotational version is reversed from that used in the other version and in SKYHOOK. For consistency it was decided to change the numbering system in the rotational version to agree with that used in the other programs. Changes had to be made in programs COORD, DIFROT, DUMBEL, ROTCOORD, and SETUP. Subroutines INITIAL, EQUIL, and LAUNCH have been added to the rotational version so that runs can be done with initial displacement in the in-plane and out-of-plane directions, and initial retrieval velocities.

In order to be able to plot the orientation of the subsatellite in various coordinate systems, the output of the program has been changed to include the rotational part of the state vector. The postprocessor has been modified to plot the orientation of the subsatellite in the rotating orbital coordinate system. This was done by adding subroutines ROTCOORD, ELEM, and ANGROT to the postprocessor which has been renamed RSTAVEC.

A second postprocessor PLOTFIL has also been modified to provide additional information. Program PLOTFIL plots the in-plane, out-of-plane and radial components of the position of the satellite. For constant wire length, the in-plane component gives a good representation of the in-plane angle. However, during retrieval the angles must be computed at each output point from the components since the wire length is constantly changing. The program has been

changed to plot the in-plane and out-of-plane angles so that the retrieval can be monitored to see if the retrieval angle is constant.

Implementation of a tension control retrieval algorithm in DUMBEL is relatively straightforward. The tension is computed in subroutine SETUP. The control laws given by equation (2.1.1) and equation (2.1.16) have been implemented with control parameters that allow various combinations of terms to be used. The program can be run in either the retrieval mode or the steady state mode. Various debugging runs were done until the program appeared to be giving correct results. One bug in particular kept making the run go unstable very quickly by applying too much tension.

2.1.3 Computer Simulations -

A set of computer simulations has been done to test the retrieval control algorithm in DUMBEL. The software modifications described in the previous section have been done concurrently with the test runs. The following parameters have been used in the runs. A 550 kg subsatellite is deployed upward on a 20 km tether from a 100 metric ton Shuttle in a circular orbit at 400 km. (Atmospheric drag is not included in these simulations, so that the results are not significantly dependent on altitude.)

An initial test run was done with rotation but the run was not completed because the integration was too slow. Using the actual moments of inertia of the subsatellite gives a relatively short period for rotation under the restoring torque of the tension in the wire. This slows down the numerical integration. The run was terminated at about 4000 seconds of orbital time with the subsatellite at 4.8 km from the Shuttle with an in-plane displacement of 12.42 degrees. Equation 2.1.16 was used without the correction for center of

mass.

Since the rotational dynamics is not necessary for studying the retrieval algorithms it was decided to put the retrieval facility into the version without rotational dynamics which has the advantage of rapid numerical integration. The first run with the program was done with the control law of equation (2.1.16) without the center of mass correction. The run was terminated at 14,800 seconds of orbital time with the subsatellite 100.9 meters from the Shuttle. The distance expected in a perfect retrieval at this time using equation (2.1.8) is 112 meters. The in-plane angle at the end of the run was 12.44 degrees. The initial conditions for the run were with the tether displaced 12.1846 degrees in the in-plane direction and a retrieval velocity of 7 meters/sec. Plots of the liberation angles showed no out-of-plane displacement, and a decaying in-plane oscillation converging to 12.44 degrees. Figure 2.1.1 shows a plot of the in-plane angle in degrees vs. time in seconds.

The second test run was done with the rotational version of DUMBEL. Since the slow integration is caused by the short period rotation of the subsatellite, the moments of inertia of the subsatellite were arbitrarily increased by a factor of 1000 in order to see if rapid integration could be achieved for the long runs required during retrieval. The run was terminated at 18,200 second with the subsatellite at 32 meters. The integration proceeded rapidly. The distance from the Shuttle expected from equation (2.1.8) is 34 meters. The final value of the in-plane angle was 11.59 degrees. A plot of the in-plane angle shows oscillations which are not damped and appear to be increasing at the end of the run. Figure 2.1.2 shows a plot of the in-plane angle in degrees vs. time in seconds. The algorithm does not at present treat the difference between the attachment point and the center of mass of the satellite in a completely rigorous manner. The rotational dynamics may be affecting the retrieval

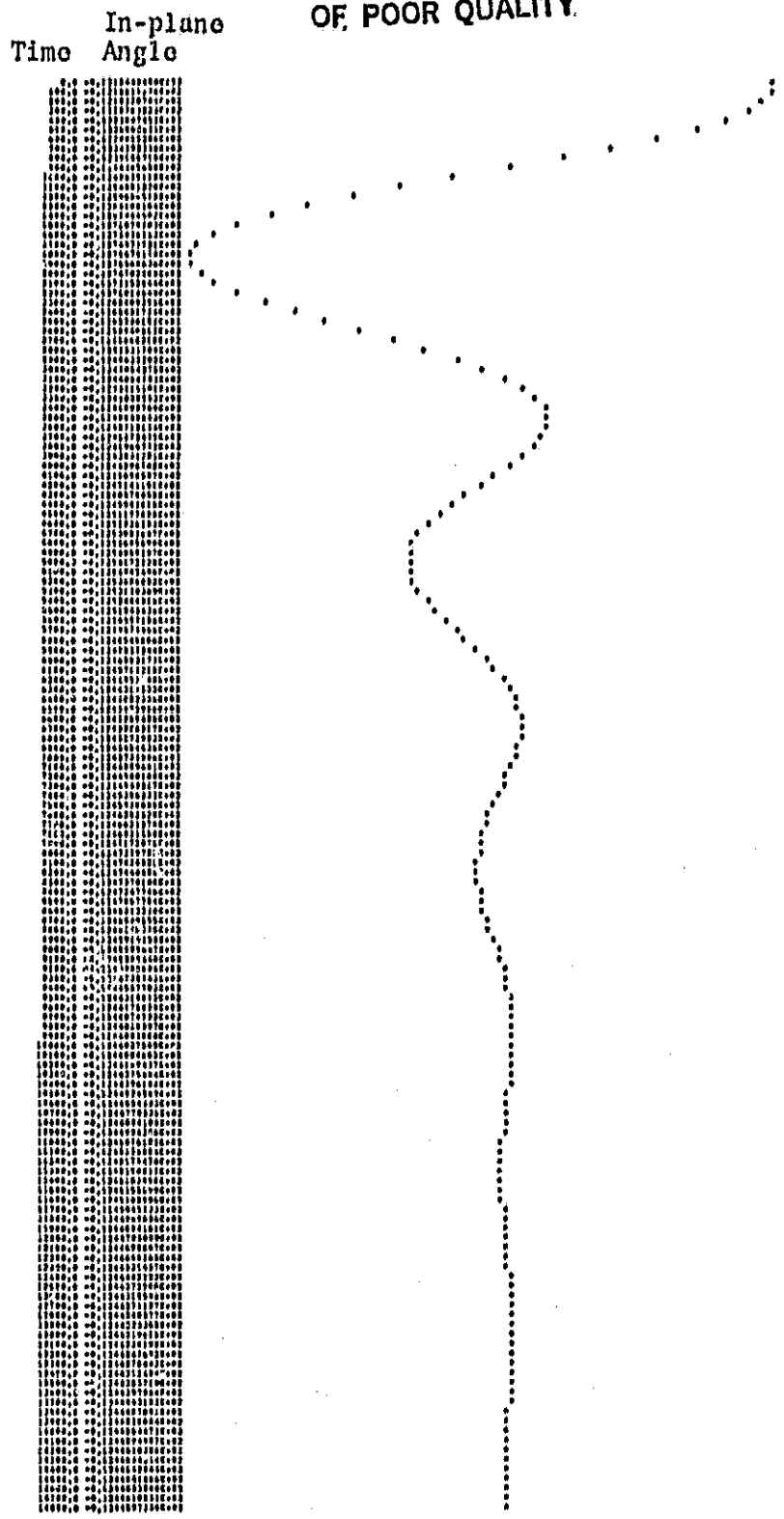

Figure 2.1.1 In-plane angle in degrees vs. time (sec.) for the first retrieval run starting from 12.18 degrees and an initial retrieval velocity of 7 m/sec.

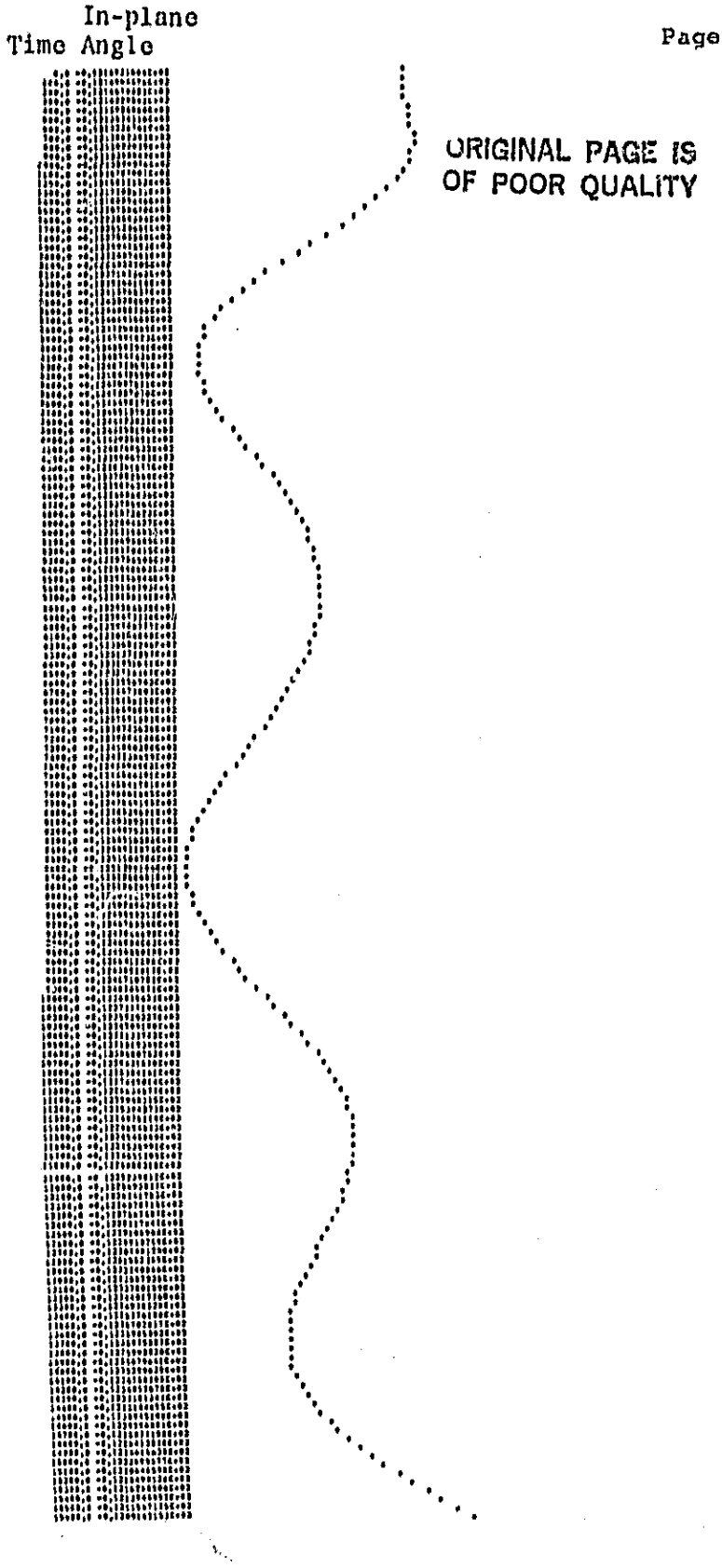

Figure 2.1.2 In-plane angle in degrees vs. time (sec.) for the second retrieval run, including rotational dynamics.

slightly.

The third test run was done using the control law of equation (2.1.1) with BOOM = 50 meters, and $\xi_d = 1$. The run went unstable and the in-plane angle reached 90° at 8500 seconds. The wire length was 1.6 km. The run was done without rotational dynamics. The initial conditions have the tether at 12.18 degrees from the vertical in the in-plane direction and an initial retrieval velocity of 7 meters/sec.

In order to test the effectiveness of the damping in the algorithm for removing initial transients, a fourth run was done starting with the wire vertical and the subsatellite stationary. The run was terminated at 21,600 seconds with the subsatellite at 11.32 meters (since the boom length = 12 meters this simulates a complete retrieval maneuver). The value calculated from equation (2.1.8) is 10.4 meters. The oscillations of the in-plane angle were well damped, decreasing by about a factor of 2 on each oscillation. The final angle was 12.44 degrees. Figure 2.1.3 shows a plot of the in-plane angle in degrees vs. time in seconds. The run was without rotational dynamics. This run was very well behaved in contrast to the third run. However the final value of the in-plane angle is clearly different from the value of 12.1846 used in computing the control law constants. The run used equation (2.1.16) without the center of mass correction.

For the fifth run, the correction factor for the center of gravity of the system was included in equation (2.1.16). The tether was initially displaced 12.18 degrees in the in-plane direction and the initial retrieval velocity was 7 m/sec. The run was terminated at 21,600 seconds with the subsatellite 10.28 meters from the Shuttle. The theoretically expected final distance is 10.42 meters. The small oscillations present initially in the in-plane angle were

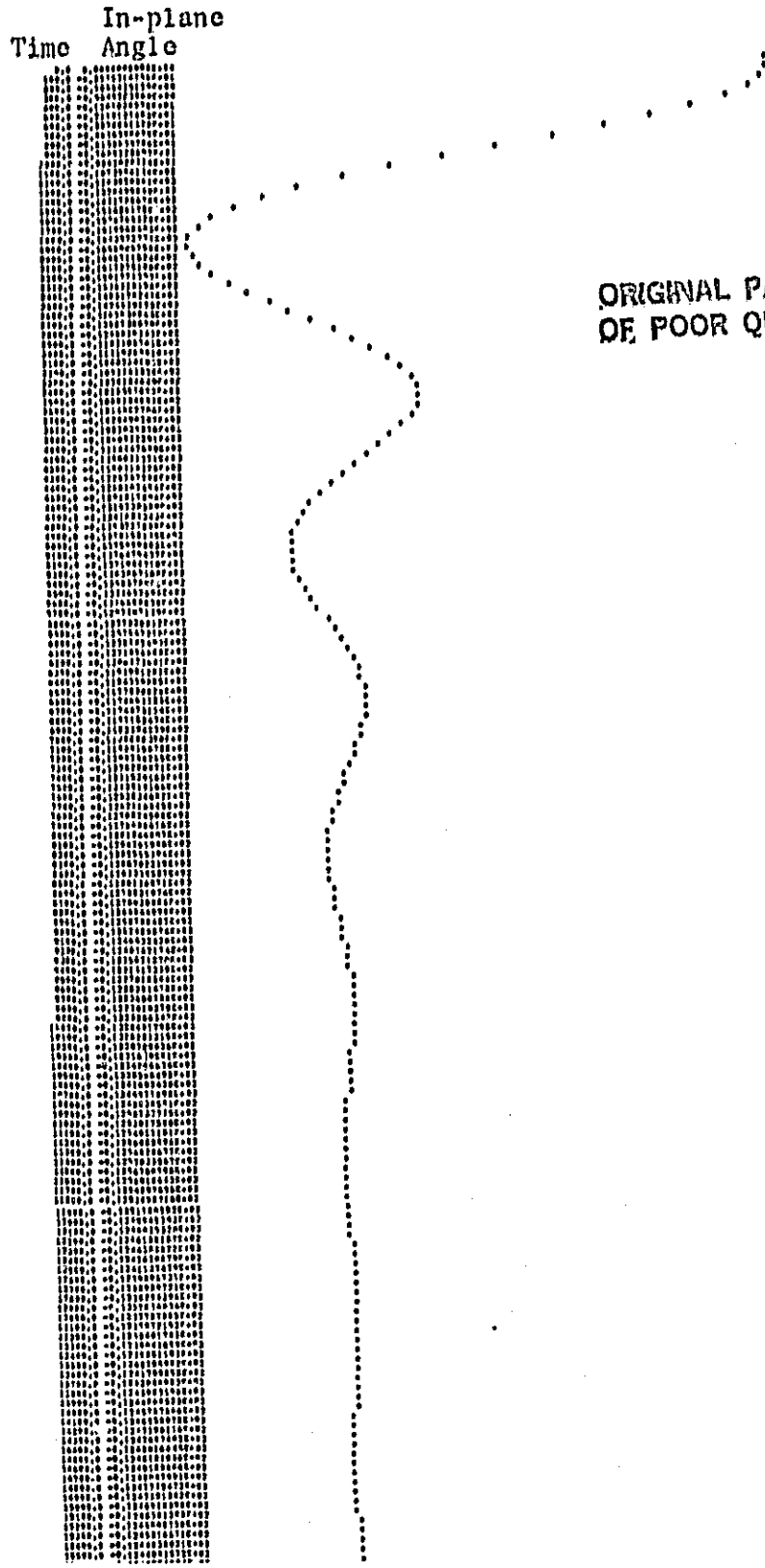

Figure 2.1.3 In-plane angle in degrees vs. time (sec.) for the fourth retrieval run starting with zero initial velocity and tether aligned with the local vertical.

well damped and the final in-plane angle was 12.1843 degrees, in close agreement with the theoretically expected value of 12.1846.

Three more test runs have been done in an effort to identify the cause of the instability in the third run. In the sixth run, equation (2.1.16) was used along with the first term of equation (2.1.1). The boom length was set to zero. Initial conditions were with the tether displaced 12.1846 degrees in-plane and an initial retrieval velocity of 7 meters/sec. The run was terminated at 10,700 seconds with a final wire length of 463 meters. The theoretical value of this time is 472 meters. The in-plane angle was stable and the final value was 12.26 degrees.

The seventh run was done with the second and third terms of equation (2.1.1) and the same initial conditions. The run was terminated at 10,100 seconds and the final wire length was 178 meters. The theoretical value is 583 meters at this time. The final angle was 17.16 degrees. It is apparent from the results that too much tension is being applied by the algorithm and the result is a too rapid retrieval with a large in-plane displacement.

The eighth run was done with the same parameters as the third run but setting the boom length equal to zero. The run was unstable at the same point as in the third run.

2.1.4 Conclusions -

The results of the computer simulations show that it is possible (neglecting effects such as atmospheric drag) to devise a control law using only length, and length rate information that will bring in the subsatellite along a straight line at a desired angle with good damping of in-plane oscillations (without any in-plane thrusters). The success of the control law depends on accurately modelling the tension necessary to keep the system in equilibrium at the desired retrieval angle. Effects that must be accounted for are the dependence of the gravity gradient on the in-plane angle, the deceleration of the subsatellite, and the position of the center of mass of the system. The control law has little effect against out-of-plane oscillations which can be handled by thrusters. The effects of atmospheric drag can also be handled by thrusters.

2.2 Implementation Of Thrusters In Rotational Dynamics Program

The TSS currently under consideration will have thrusters in the in-plane, out-of-plane, and in-line directions, and another thruster for controlling rotation about the vertical axis of the satellite. It is assumed that the tension in the wire will align the subsatellite attitude along the direction of the wire. The thrusters will be used to control librations during retrieval. In order to implement the thruster algorithms it is necessary to construct unit vectors in the direction of firing of the thrusters and calculate the swing velocities in the in-plane and out-of-plane directions.

2.2.1 In-Plane And Out-Of-Plane Unit Vectors -

There are a number of coordinate systems involved in simulating the use of thrusters on-board the subsatellite. The position, velocity, and orientation of the subsatellite, and the position and velocity of the Shuttle are integrated in inertial coordinates. Since the thrusters are attached to the subsatellite, the direction of firing is specified by the direction cosine matrix giving the subsatellite orientation. For this initial analysis it is assumed that the orientation of the subsatellite is controlled so that the thrusters point in the in-plane, out-of-plane, and in-line directions.

The first task is to construct unit vectors in the direction of the thrusters. If $\vec{P}_1$ and $\vec{V}_1$ are the position and velocity of the Shuttle, the normal to the orbit is

$$\vec{N} = \vec{P}_1 \times \vec{V}_1 \qquad (2.2.1)$$

The direction of the wire is

$$\vec{w} = \vec{P}_2 - \vec{P}_1$$

where $\vec{P}_2$ is the position of the subsatellite. The direction of the in-plane thruster is given by

$$\vec{U}_{IN} = \vec{N} \times \vec{w}.$$

The out-of-plane vector is

$$\vec{U}_{OUT} = \vec{w} \times \vec{U}_{IN}$$

2.2.2 Libration Velocity Of The Subsatellite -

The objective of the use of thrusters during retrieval is to eliminate librations that could build up and cause unstable behavior. The input to the control algorithm is the libration velocity. In order to calculate this quantity it is necessary to know what the velocity of the subsatellite would be in inertial space if the subsatellite were not librating. The difference between this and the actual velocity is then the libration. The components of this velocity along the in-plane and out-of-plane vectors give the in-plane and out-of-plane libration velocities.

If there is no libration, the whole tethered system rotates like a rigid body with the normal to the orbit as the axis of rotation. The unit vector normal to the orbit is

$$\hat{n} = \vec{N}/|\vec{N}|$$

where $\vec{N}$ is given by equation (2.2.1). The velocity of the subsatellite is in the direction

$$\vec{Q} = \hat{n} \times \vec{P}_2$$

The radius of rotation of the subsatellite is

$$\rho_2 = |\vec{Q}|$$

The radius of rotation of the Shuttle is

$$\rho_1 = |\vec{P}_1|$$

and the velocity of the Shuttle is

$$v_1 = |\vec{V}_1|.$$

The ratio of the subsatellite velocity to the Shuttle velocity is ρ_2/ρ_1 without libration. For a circular orbit the velocity of the subsatellite should be in the direction of $\vec{Q}$. However, in an eccentric orbit, there will be a radial component of the velocity except at perigee and apogee. In an eccentric orbit there is no uniformly rotating orbital reference frame so that it is not clear what the velocity of the subsatellite should be without libration. However, in an attempt to define an approximate rotating reference system, the radial velocity of the Shuttle has been accounted for in calculating the direction of the subsatellite velocity without libration. The angle by which the Shuttle velocity deviates from that of a perfect circular orbit is approximately

$$\alpha = \vec{P}_1 . \vec{V}_1 / (\rho_1 v_1)$$

The unit vector for the direction of the subsatellite velocity is then constructed as

$$\hat{q} = \vec{Q}/\rho_2 + \alpha \vec{P}_1/\rho_1$$

The magnitude of the velocity of the subsatellite is

$$v_2 = v_1 \rho_2/\rho_1$$

so that the vector velocity for the subsatellite without libration is

$$\vec{v}_2 = v_2 \hat{q}.$$

The libration velocity is then

$$\Delta \vec{V}_2 = \vec{V}_2 - \vec{v}_2$$

where V_2 is the actual velocity of the subsatellite. The in-plane component of the libration is

$$V_{IN} = \Delta\vec{V}_2 \cdot \vec{U}_{IN}$$

and the out-of-plane component is

$$V_{OUT} = \Delta\vec{V}_2 \cdot \vec{U}_{OUT}$$

There will of course also be a radial component of $\Delta\vec{V}$ but this is not needed for the thruster control algorithm.

2.2.3 Software Implementation Of Coordinate Systems For Thruster Algorithms -

The equations developed in sections 2.2.1 and 2.2.2 have been coded in subroutine INOUT (Z, DV, T, WIRE, UIN, UOUT), when Z is the state vector for the Shuttle and subsatellite, DV is the libration velocity in inertial coordinates, T is the time, and WIRE, UIN and UOUT, are unit vectors in the radial, in-plane, and out-of-plane directions.

A calling program has been written to read Z and call INOUT for testing purposes. A debugging version of the program was written to print the various vectors computed. Tests have been done with no libration angle, an in-plane and an out-of-plane displacement of the subsatellite for a circular orbit. All quantities have been checked against hand calculations. The tests have been repeated with a slight eccentricity to see that the vectors change in an appropriate manner.

Since the tests of the subroutine seemed satisfactory the subroutine was put into the DUMBEL program. It is called from subroutine DIFFUN which computes the time derivative of each component of the state vector of the system. A number of test runs have been done and the debugging print examined to make sure the results are reasonable. The first test run was with no libration. The

differential velocity was zero as it should be. Runs were done with an in-plane displacement only, and an out-of-plane displacement only, in an equatorial orbit. The DUMBEL program has a simplified facility for setting up initial libration angles written for equatorial orbits only. A test run was done at 28° inclination with no libration. The differential velocity was zero as it should be. A final run was done at a 45° orbital inclination with an in-plane displacement introduced manually in the initial conditions. The output shows an in-plane component of the differential velocity, no out-of-plane component and a slight radial component.

2.2.4 Critical Damping Of Librations With Thrusters -

For a simple harmonic oscillator the critical damping coefficient is $2m\omega$, where ω is the frequency and m is the mass. For in-plane librations, the frequency of oscillation is $\sqrt{3}\omega_o$ where ω_o is the orbital frequency. For out-of-plane oscillations $\omega = 2\omega_o$. The critical damping coefficients are therefore

$$b_{IN} = 2m_2\sqrt{3}\omega_o$$

and

$$b_{OUT} = 2m_2 2\omega_o = 4m_2\omega_o.$$

The thrust required to provide critical damping is, for each component,

$$F_{IN} = -b_{IN}\, V_{IN}$$

$$F_{OUT} = -b_{OUT}\, V_{OUT}.$$

2.2.5 Computer Simulations Of Thrusters For Critical Damping -

A couple of test runs have been done using the algorithms for critical damping. In the first run the tether was given an out-of-plane displacement of 10 degrees. The simulation was run for 5000 seconds. The out-of-plane displacement approached the rest position exponentially without overshooting. The times corresponding to 10°, 1°, .1° and .01° were 0, 1700, 2900, 4100 seconds. The amplitude decays by a factor of ten every 1200 seconds. Because of the coupling between the in-plane and out-of-plane angles, the out-of-plane motion induced an in-plane oscillation of about ±.8°. This in-plane oscillation was not damped. Fig. 2.2.4 shows the out-of-plane angle vs. time, and Fig. 2.2.5 shows the in-plane angle vs. time.

In the second test run, the tether was given an in-plane displacement of 10°. There was no out-of-plane oscillation as expected, since the in-plane oscillation does not couple to the out-of-plane as long as the out-of-plane displacement is zero. The in-plane angle returned exponentially to zero. The times when the angle was 10, 1, .1 and .01 degrees were 0, 200, 3400, and 4800 seconds. The time to decay by a factor of 10 is about 1400 seconds. Figure 2.2.6 shows the in-plane angle vs. time.

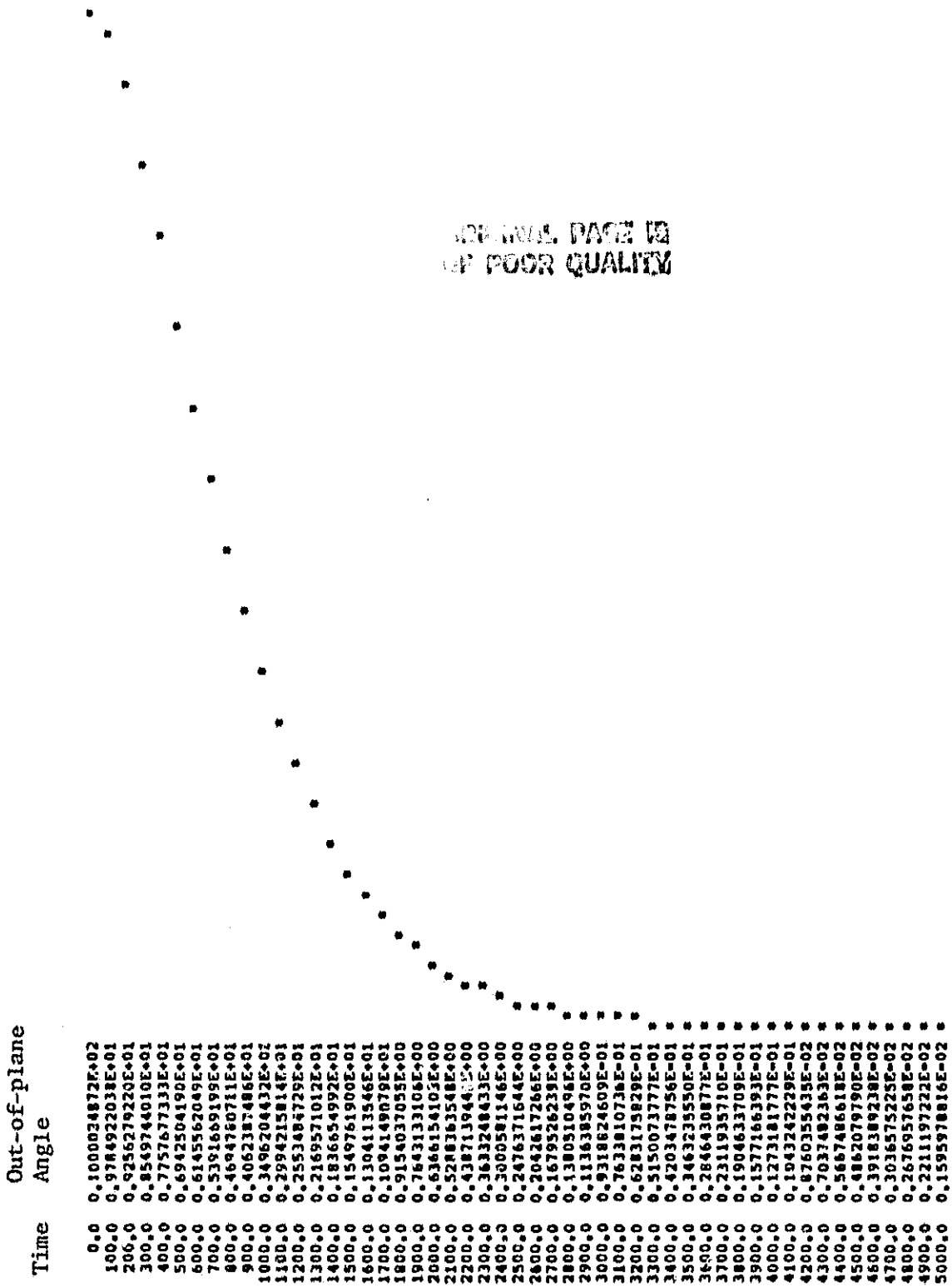

Time	Out-of-plane Angle
0.0	0.10000348726+02
100.0	0.97869220386+01
200.0	0.92562792206+01
300.0	0.85497440106+01
400.0	0.77576773336+01
500.0	0.69425041906+01
600.0	0.61455620496+01
700.0	0.53916691996+01
800.0	0.46947607116+01
900.0	0.40623874866+01
1000.0	0.34962044326+01
1100.0	0.29942158146+01
1200.0	0.25534867296+01
1300.0	0.21695710126+01
1400.0	0.18366549926+01
1500.0	0.15497619006+01
1600.0	0.13041135466+01
1700.0	0.10941480796+01
1800.0	0.91540370556+00
1900.0	0.76431331066+00
2000.0	0.63615410366+00
2100.0	0.52863535886+00
2200.0	0.43871194456+00
2300.0	0.36332484336+00
2400.0	0.30058114656+00
2500.0	0.24763716446+00
2600.0	0.20426172666+00
2700.0	0.16795262396+00
2800.0	0.13805104966+00
2900.0	0.11363859706+00
3000.0	0.93188246096-01
3100.0	0.76338107386-01
3200.0	0.62831758296-01
3300.0	0.51500737776-01
3400.0	0.42034787566-01
3500.0	0.34632355506-01
3600.0	0.28464308776-01
3700.0	0.23119357106-01
3800.0	0.19006337096-01
3900.0	0.15771663936-01
4000.0	0.12731817776-01
4100.0	0.10432422296-01
4200.0	0.87603554356-02
4300.0	0.70374823636-02
4400.0	0.56674866186-02
4500.0	0.48620797906-02
4600.0	0.39183892386-02
4700.0	0.30365752256-02
4800.0	0.26769576586-02
4900.0	0.22111972226-02
5000.0	0.15959788166-02

Figure 2.2.4 Out-of-plane angle (degrees) vs. time (sec.) starting with a 10° out-of-plane displacement and using the out-of-plane thrusters for critical damping.

Time	Out-of-plane Angle
0.0	0.10000248727E+02
100.0	0.97849220388E+01
200.0	0.92562792220E+01
300.0	0.85497440103E+01
400.0	0.77576773393E+01
500.0	0.69425041905E+01
600.0	0.61455620495E+01
700.0	0.53916691995E+01
800.0	0.46947807116E+01
900.0	0.40623884886E+01
1000.0	0.34962044328E+01
1100.0	0.29942158146E+01
1200.0	0.25534864729E+01
1300.0	0.21695710126E+01
1400.0	0.18365499926E+01
1500.0	0.15497619908E+01
1600.0	0.13041135468E+01
1700.0	0.10941490780E+01
1800.0	0.91540370558E+00
1900.0	0.76431331068E+00
2000.0	0.63615410368E+00
2100.0	0.52883635488E+00
2200.0	0.43871139448E+00
2300.0	0.36332488433E+00
2400.0	0.30058811468E+00
2500.0	0.24763716448E+00
2600.0	0.20426172668E+00
2700.0	0.16795262398E+00
2800.0	0.13805104968E+00
2900.0	0.11383859708E+00
3000.0	0.93886246098E-01
3100.0	0.76398107368E-01
3200.0	0.62811759298E-01
3300.0	0.51500737778E-01
3400.0	0.42034787568E-01
3500.0	0.34632355508E-01
3600.0	0.28464308778E-01
3700.0	0.23193571078E-01
3800.0	0.19046337098E-01
3900.0	0.15571663938E-01
4000.0	0.12731817778E-01
4100.0	0.10432422298E-01
4200.0	0.87603554358E-02
4300.0	0.70374823638E-02
4400.0	0.56674866188E-02
4500.0	0.48620797908E-02
4600.0	0.39138923888E-02
4700.0	0.30357522258E-02
4800.0	0.26769576588E-02
4900.0	0.22111972228E-02
5000.0	0.15959788168E-02

Figure 2.2.4 Out-of-plane angle (degrees) vs. time (sec.) starting with a 10° out of plane displacement and using the out of plane thrusters for critical damping.

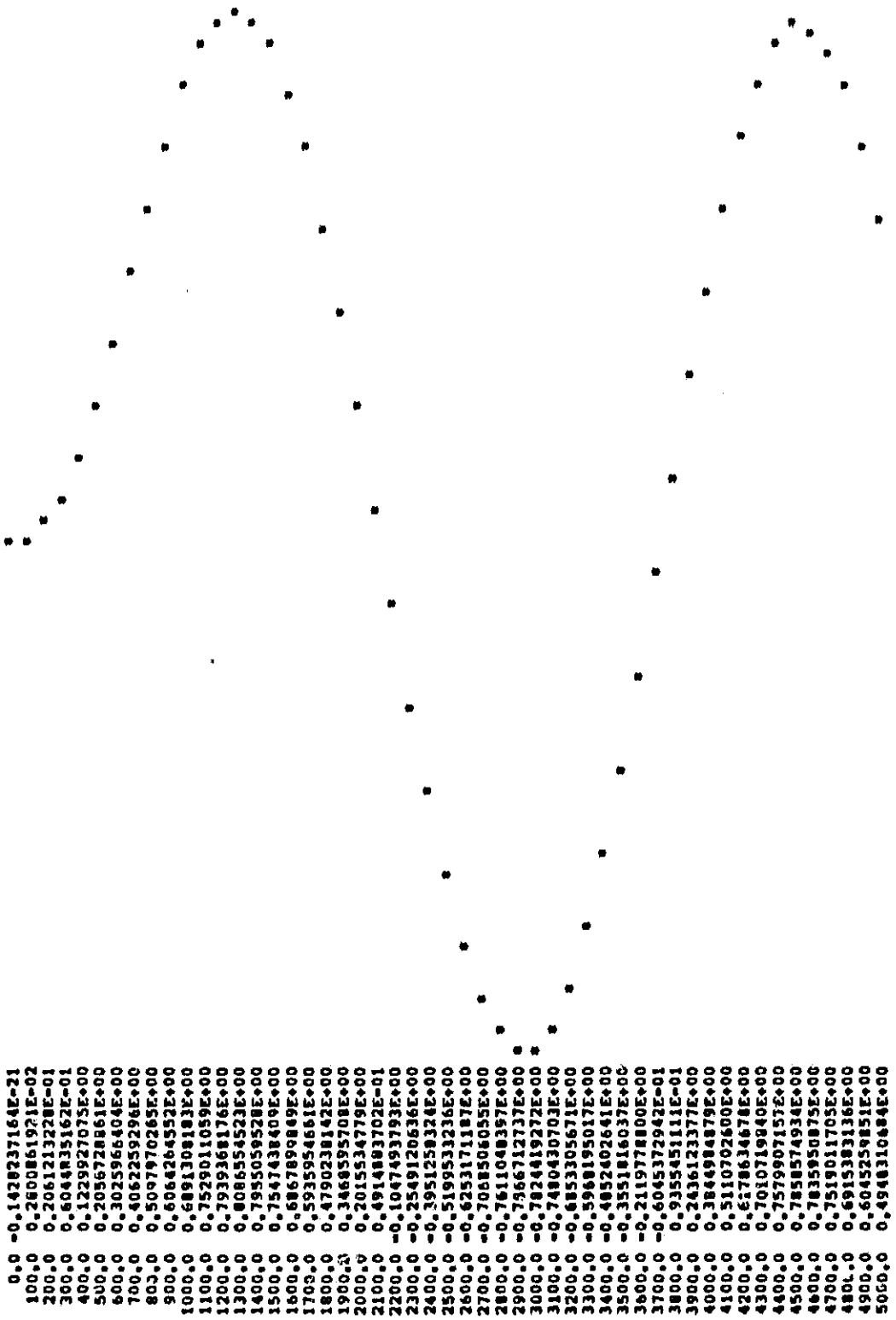

Time	In-plane Angle
0.0	-0.142837164E-01
100.0	0.260086192IE-02
200.0	0.206121322BE-01
300.0	0.604483516ZE-01
400.0	0.122992707SE+00
500.0	0.205672886IE+00
600.0	0.302596640AE+00
700.0	0.406225929GE+00
800.0	0.509770265E+00
900.0	0.606426455ZE+00
1000.0	0.689130818JE+00
1100.0	0.752901105GE+00
1200.0	0.793936817GE+00
1300.0	0.808655452JE+00
1400.0	0.795505952BE+00
1500.0	0.754743840GE+00
1600.0	0.686789984GE+00
1700.0	0.593554661E+00
1800.0	0.479023814ZE+00
1900.0	0.346859570BE+00
2000.0	0.201553477GE+00
2100.0	0.491488370ZE-01
2200.0	-0.104793793E+00
2300.0	-0.254912063GE+00
2400.0	-0.395125832AE+00
2500.0	-0.519953336E+00
2600.0	-0.625317118ZE+00
2700.0	-0.706850605SE+00
2800.0	-0.761104835ZE+00
2900.0	-0.786712737E+00
3000.0	-0.782419272E+00
3100.0	-0.748043070JE+00
3200.0	-0.685330567IE+00
3300.0	-0.596819501ZE+00
3400.0	-0.485240264IE+00
3500.0	-0.355181603ZE+00
3600.0	-0.211977880E+00
3700.0	-0.604537294ZE-01
3800.0	0.935545111IE-01
3900.0	0.243612337TE+00
4000.0	0.384498487BE+00
4100.0	0.511070260DE+00
4200.0	0.617863467BE+00
4300.0	0.701071984OE+00
4400.0	0.757907157E+00
4500.0	0.785857493HE+00
4600.0	0.783595087SE+00
4700.0	0.751901170SE+00
4800.0	0.691538313GE+00
4900.0	0.604525985IE+00
5000.0	0.494831068HE+00

Figure 2.2.5 In plane angle (degrees) vs. time (sec.) starting with a 10° out-of-plane displacement and using the out-of-plane thrusters for critical damping.

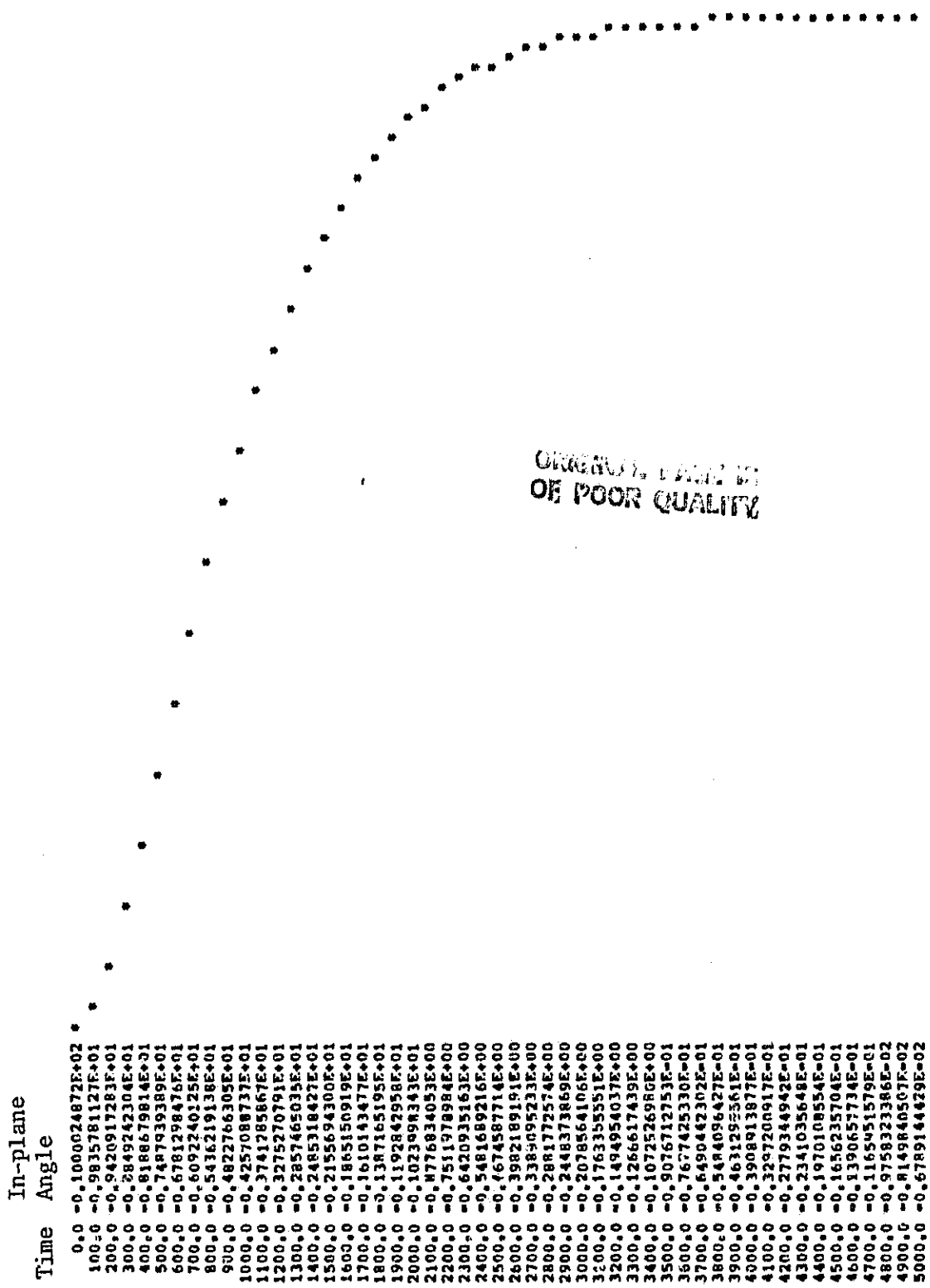

Figure 2.2.6 In-plane angle (degrees) vs. time (sec.) starting with a 10° in-plane displacement and using the in-plane thrusters for critical damping.

2.3 Slack Tether Studies

The slack tether simulation program SLACK3 has been enhanced to make the three dimensional version fully usable, and to improve handling of difficult cases. Several case studies have been run and are presented here.

The influence of tether viscous damping is examined and found to be possibly significant, both for the physical tether and our attempts to model it.

2.3.1 Slack3 Modification And Utilization -

During the reporting period SAO has enhanced and modified the SLACK3 slack tether simulation program. A series of case studies suggested by Mr. C. C. Rupp of NASA were run. Difficulties encountered with these runs led to further modifications to the bounce handling routines.

2.3.1.1 Program Modifications And Enhancements -

As features (such as boom rotation) were added to SLACK3, the number of input parameters increased also, until the arcane input procedure required approached in complexity that of SKYHOOK. In particular, interactive runs involved a long dialogue with much room for operator error and frustration. In the current version of SLACK3, a set of lexical routines developed for SKYHOOK (under NASA Grants NAG5-325 and NAG5-458) were used to create a "menu": most parameters now have default values (e.g. a 1/2 tonne subsatellite, deployed upward 20 km) which are displayed initially; if the user wishes to change, say, the angle at which the tether is deployed she will then enter and identifier "tether.angle"; if the identifier is followed by the appropriate number of

parameters (e.g. "tether.angle -35.0 0.0") they are accepted, and otherwise the program prompts for the specific quantities. In addition to being "user friendly" for interactive use, this structure makes the input file for batch processing much more readable, since each non-default parameter is clearly identified. Most input is also done in appropriate units, e.g. km instead of cm, degrees instead of radians. The tether properties can be entered either as simple material properties (such as E) or as specific tether properties (AE).

Other enhancements to SLACK3 are:

- The boom origin need no longer be at the Shuttle center of gravity. An (x,y,z) may be specified.
- Thrusters on board the Shuttle may be fired. Rather than "operating" the Shuttle's particular thruster configuration, the user must specify an acceleration value, direction and initiation time.

In addition to the enhanced features, several modifications were made to SLACK3 to avoid "infinite loop" type situations encountered while running the case studies described below. Some of these studies involved, for instance, long time scales for which the program had not been tested and which led to problems with the machine roundoff. The root finding routine, REFINE, was made substantially more robust: the interval error tolerance is checked to ensure that it is not smaller than the machine's precision (a problem possible to run into when using an absolute input tolerance and the time value becomes larger than previously experienced); corrective action is taken if the interval does not shrink; and as a last resort, the problem is solved with the inefficient but infallible bisection method (the major algorithm is modified regular falsi). The method of choosing the left (early) limit of the interval containing the root in BOOMTIME was analyzed and modified to avoid the occasional case where an interval not containing the root was chosen (due to roundoff, root-finder

truncation, etc.) when finding the next bounce between the boom and mass 1 after a given such bounce; the default left limit in such a case is the actual bounce time, and small errors make this time not specifiable precisely so that one must check and occasionally adjust this left limit. One case study, which as discussed below is actually physically unsuitable for SLACK3 simulation, still leads to an infinite loop type of failure; though this is a symptom of the underlying physics, we shall attempt to improve the program so as to avoid outright failure.

2.3.1.2 Case Studies Of Tether Break Situations -

At the suggestion of Mr. C. C. Rupp of NASA, we have used SLACK3 to study several specific examples of operational interest. All cases involved an electrodynamic tether deployed straight up, with the boom deployed 35° backward from vertical. No avoidance maneuvers (rotation, thrusters) were made. Tether properties of d = 0.3 cm, μ = 0.08 g/cm, and AE = 0.6 x 10^{10} dynes were used; the damping was set to zero since the correct value is uncertain and damping may have serious ramifications for the SLACK3 model (see Section 2.3.2 below). The initial configurations were slightly perturbed, the same relative perturbations being employed in each case. Each case was run for approximately the same physical time relative to a crude time scale defined by the cut length divided by the recoil velocity.

Two series of cases were simulated: First, a set with the tether fully deployed to 20 km and severed at 1, 10 and 20 km. Second, breaks at 0.5 km from the Shuttle with original deployed tether lengths of 1 km, 10 km and 20 km. For the 1 km original tether, a 2 Newton thruster was included by using a tension "fudge factor" of 2.0 (since the gravity gradient tension is about 2.08 N)

doubling the recoil velocity.

The results of these simulations are shown in Figures 2.3.1 through 2.3.5, in the familiar SKYHOOK side-view and front-view series of snapshots.

In Figure 2.3.1, the 20/1 case (20 km deployed tether cut at 1 km from the Shuttle), the recoil velocity is relatively rapid, and we see that initially the tether is brought forward of the Shuttle by Coriolis force, largely missing the Shuttle; after passing the Shuttle and becoming extended in the downward direction, air drag forces and an overall "bounce" from the initial forward direction take over and the configuration becomes trailing. It is not clear whether this trailing position is permanent or whether there will be another overall bounce bringing the tether back forward to impinge on the Shuttle; one case described in the first quarterly report indicated that for at least some tether lengths the trailing position is stable. If of interest, this case could be carried further.

The behavior shown in Figure 2.3.2, the 20/10 case, is surprisingly different. The tether crumples up slightly on recoil, then gravity gradient forces take effect and straighten it out again only to have the elastic tether "bounce" back in a second recoil, and so forth. The simulation did not go nearly as far relative to the recoil time scale as that in Figure 2.3.1 because the attempts to come into tension at the overall "bounces" greatly increase the number of ball-and-spring bounces which in turn determines the computational effort; this case terminated on exceeding a cpu time limit. The Shuttle is clearly safe from the vast majority of the tether in this case, since most of it does not have the energy to overcome the gravity gradient force, but it could become entangled with the portion near itself. This might be clarified by a simulation with segments strongly bunched in the region near the Shuttle, and a

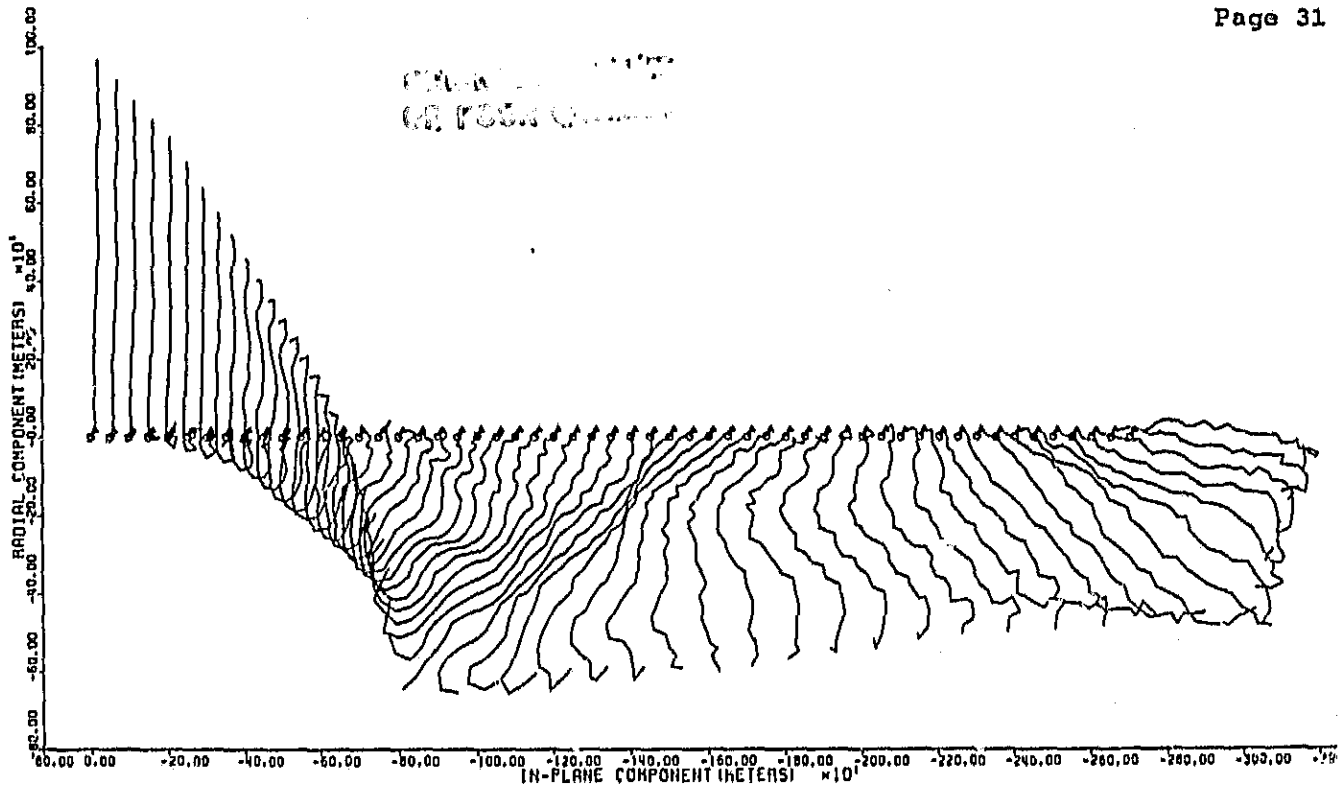

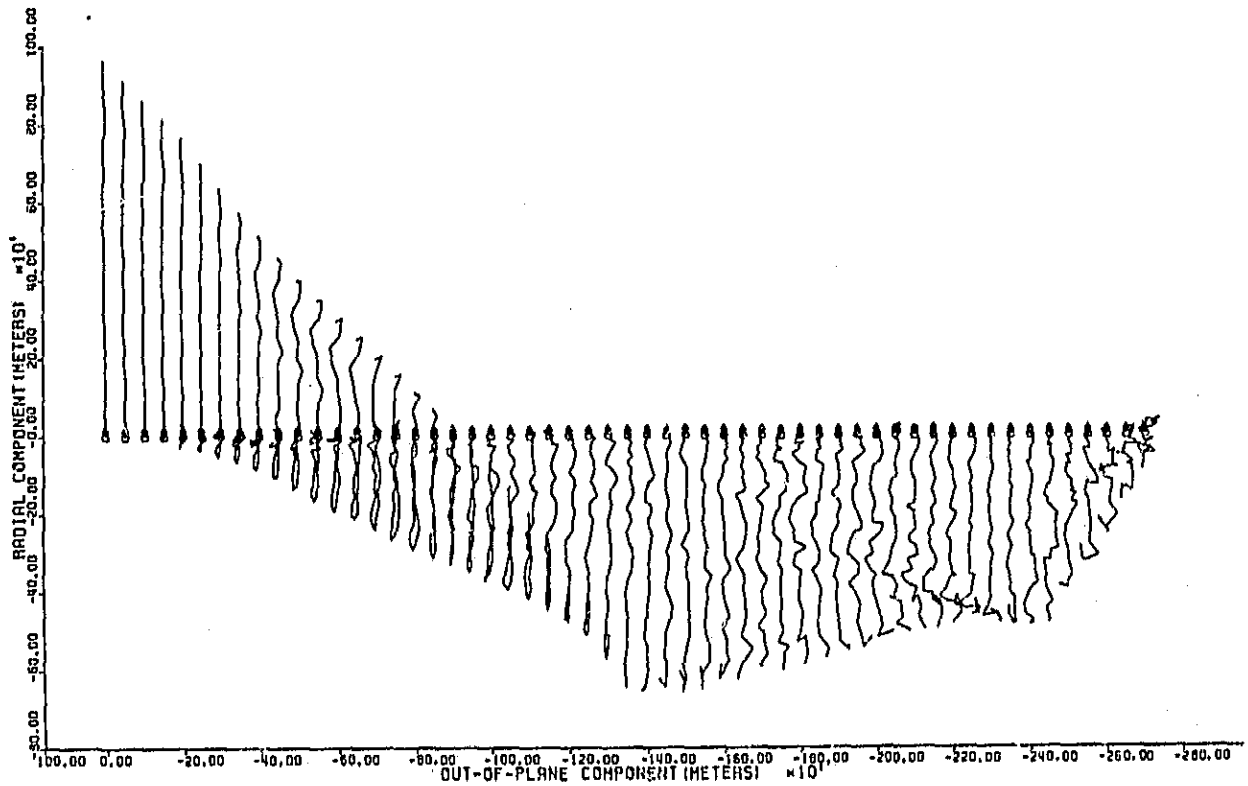

Figure 2.3.1. 20 km tether cut at 1 km. Output at 25 second intervals, total run of 1350 sec.

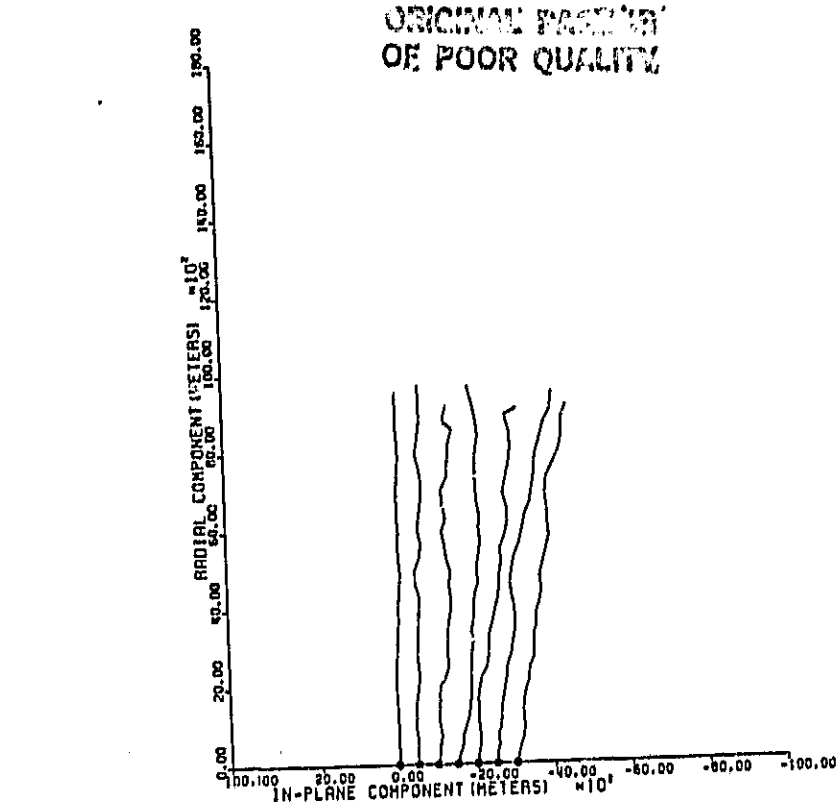

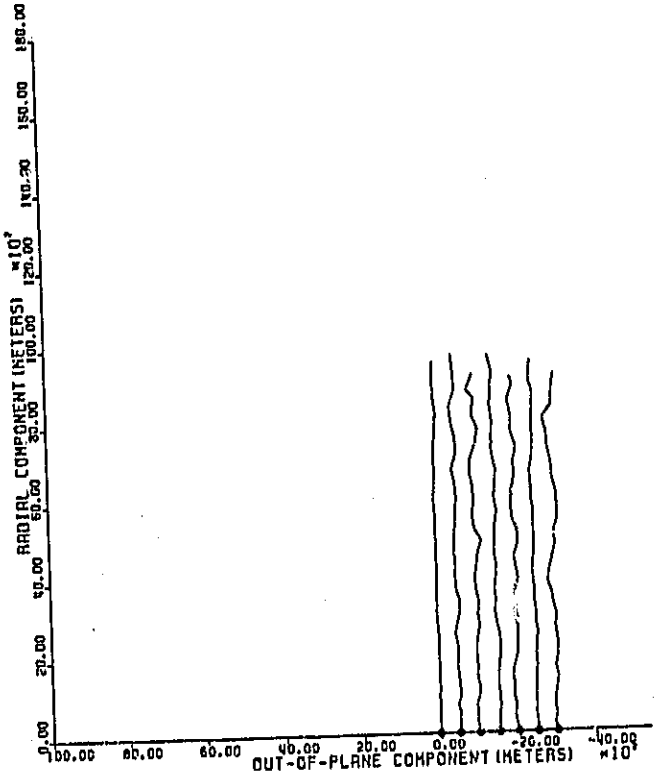

Figure 2.3.2. 20 km tether cut at 10 km. Output at 250 second intervals, total run of 1500 sec.

modification of the plot routine to allow plotting only the first few segments.

There is no figure for the 20/20 case. The bouncing behavior due to insufficient recoil velocity noticed in the 20/10 case would be, of course, even more pronounced, and led to an infinite bounce cycle. This failure is being studied, but the overall behavior should be about as in the 20/10 case.

Figure 2.3.3 shows the 20/.5 case. This is similar to the 20/1 case, with the same recoil velocity but even less tether remnant. The overall forward contribution of the Coriolis force is not so pronounced (since it does not have as much time in which to act), hence neither is the rearward bounce; the drag also does not have as much time in which to act. Figure 2.3.4, the 10/.5 case, is similar, with less forward Coriolis (hence less bounce back) and more drag, due to the decreased velocity and lengthened time scale. Interaction with the Shuttle is not clear in either case but seems likely.

Figure 2.3.5, the 1/.5 case, shows the result of a comparatively slow recoil: drag dominates completely. At least for the initial recoil the tether stays as clear of the Shuttle as one could desire, though there is some indication that the tether may bounce forward, leading to impact. This case terminated due to excess cpu time: the dominant drag tends to bring the tether into tension, leading to frequent ball-and-spring bounces.

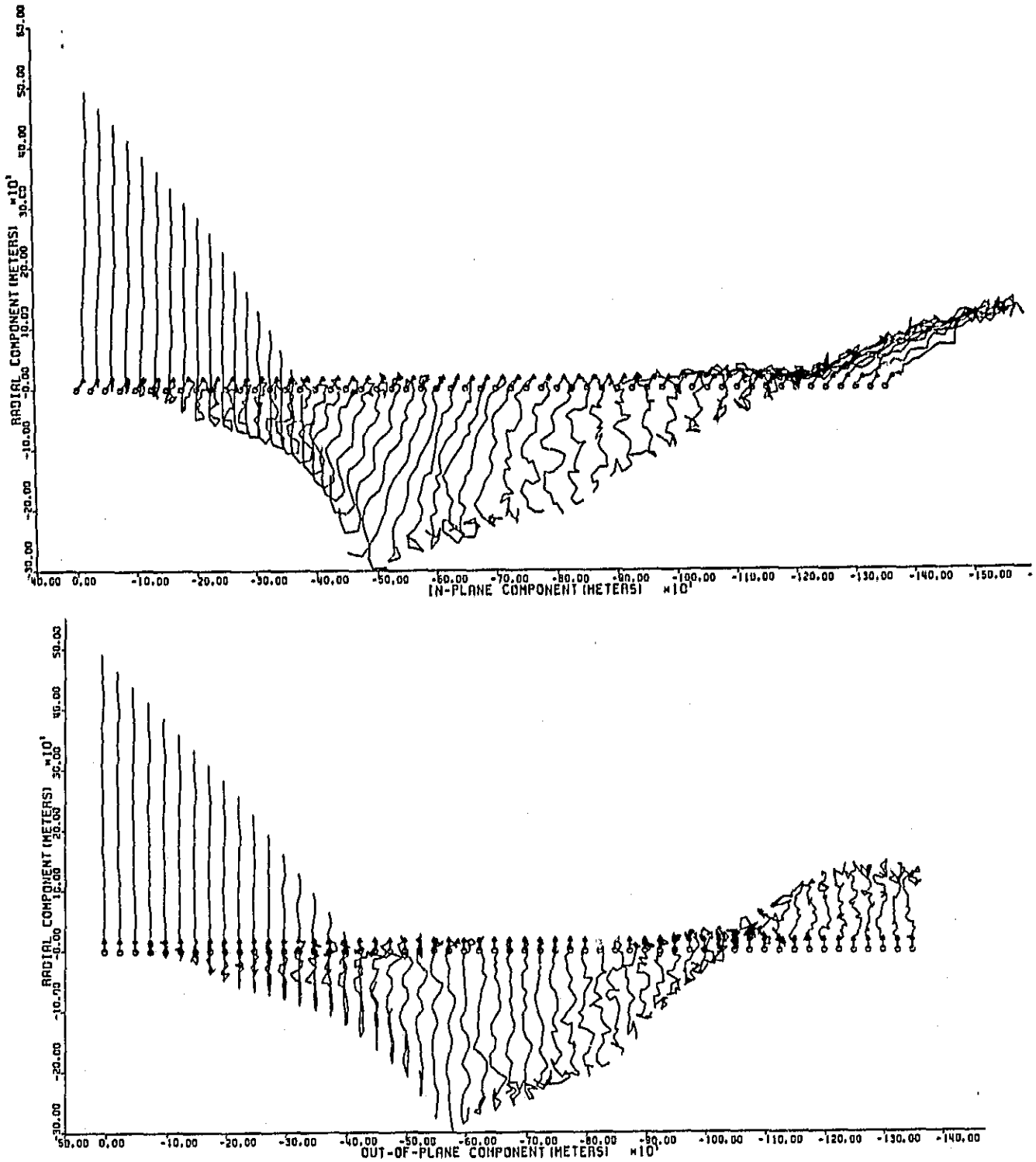

Figure 2.3.3. 20 km tether cut at 0.5 km. Output at 12.5 second intervals, total run of 675 sec.

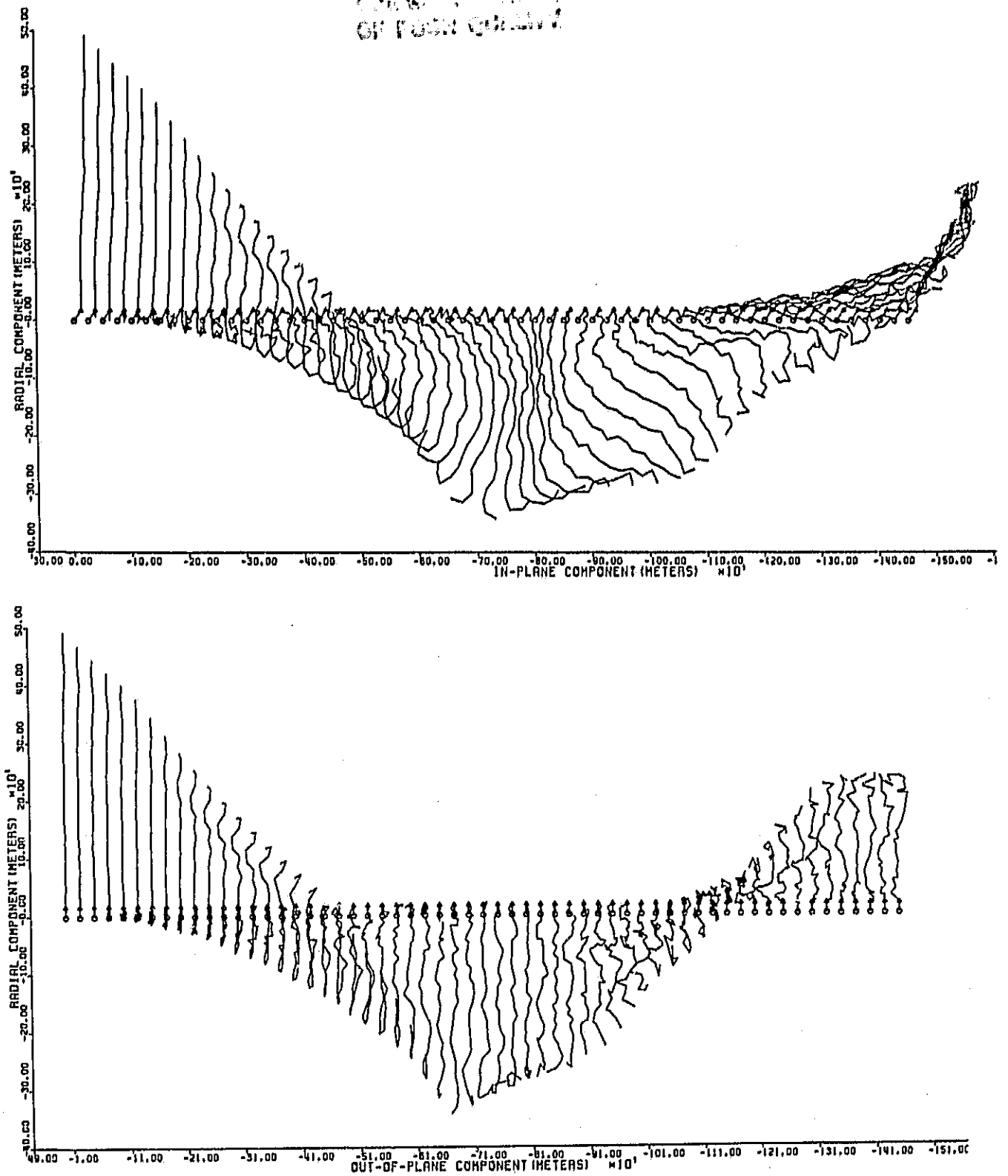

Figure 2.3.4. 10 km tether cut at 0.5 km. Output at 25 second intervals, total run of 1450 sec.

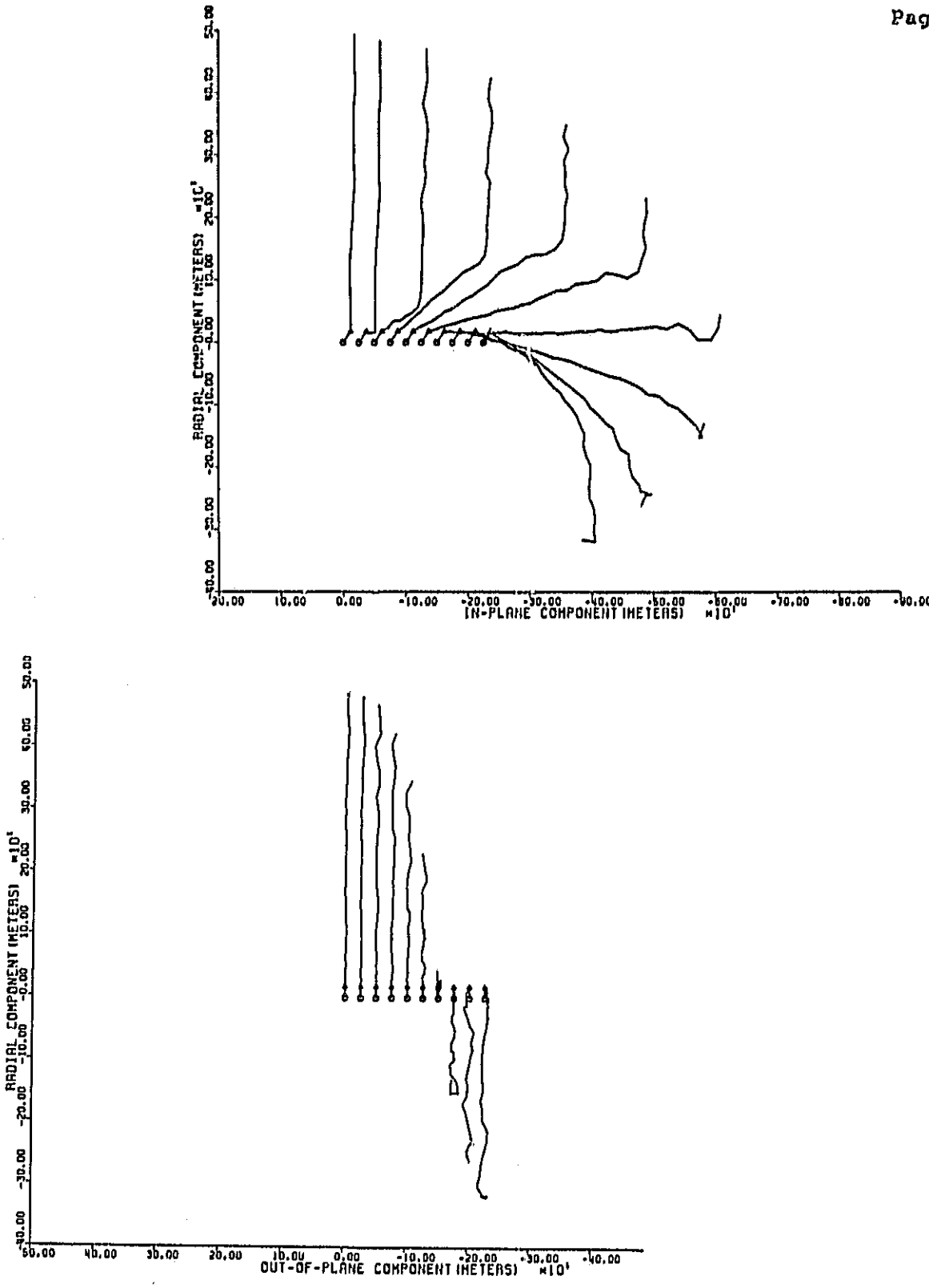

Figure 2.3.5. 1 km tether cut at 0.5 km; 2 Newton thruster on before break. Output at 125 second intervals, total run of 1125 sec.

2.3.1.3 Failures And Difficult Cases: Implications For The Model -

Those cases which either failed or took inordinate amounts of computer time due to large numbers of bounces, both in the above simulations and from previous experience, tend to be those cases in which one expects the tether to be brought into tension, as by gravity gradient or drag forces. The reason is simple: SLACK3 assumes that all the segments joining it's component masses are slack, except at infinitesimally short "bounces." When the physical situation requires that the (continuous, physical) tether becomes taut and stretches for some finite time, the program can only try to approximate this by placing the ball-and-spring bounces closer and closer together. Sometimes it appears to make a reasonable approximation, as when the tether whips past the Shuttle and rebounds at the opposite extension, but other cases simply prove too difficult. (One might also harbor doubts about these seemingly well handled cases, although the physically appealing behavior of the simulations lends some confidence.)

Initially, we had hoped that it might be possible to handle the cases in which segments remain in tension for finite periods, within the same ball-and-spring model. It now appears that adequate numerical/analytical handling of the tensioned case would not only be a major programming task but would be computationally expensive. The number of masses required for realistic simulations (thirty or more) and the large number of bounces (into and out of tension) occupy substantial, though not prohibitive, computer time when the only calculations are simple root finding and free trajectory calculation. Taut tether calculations, which would involve either integrating sets of differential equations directly or eigensolutions to large (though sparse) non-symmetric matrices which would keep changing in form and size as segments come into and out of tension, is likely to be much more expensive. Some imprecise, but perhaps reasonable, approaches to including taut segments at least crudely have

been suggested and may be tried if they seem feasible after further examination.

It is interesting to note the following: our assumption of a completely free tether recoil leads to a configuration on loss of tension in which the tether is travelling with a uniform velocity and is extended to just its natural length. Immediately, at one end it interacts with the deployment boom, but throughout the tether the gravity gradient forces act to stretch the tether and bring it uniformly, immediately and simultaneously into tension. (This was a primary influence behind introducing randomization into the simulation.) Indeed, it should have been tensioning the tether immediately behind the wave of detensioning. Physically, of course, we know this will not happen in such a clean and immediate fashion; this is an artifact of turning on the forces only after the idealized elastic recoil. The initial loss of tension process seemingly needs further study with the gravity gradient, and possibly Coriolis and drag, forces taken into account.

2.3.2 Tether Properties And Implications -

Viscous damping in the tether has not been given the attention it deserves. In general, this damping determines a wavelength below which tether oscillations cannot be sustained. More particularly, with regard to the SLACK3 model, it also defines a segment size below which the damping forces dominate the ball-and-spring bounce forces which SLACK3 primarily deals with; including damping approximately is insufficient if it is so severe that a pair of masses will never exit from a bounce between them. As we shall see below, it appears that for some not untypical cases (e.g. 30 segments for a 500 meter tether remnant) the segment length is comparable to the wavelength for critical damping.

To have a handy intuitive summary figure, one related to the internal dynamics of the tether which are the current focus of our work, define a "wavelength for critical damping" of longitudinal tether oscillation modes: $W_{CRIT} = \pi C_V / \sqrt{\mu AE}$. This is found by applying the damped wave equation to a system with fixed boundary conditions at 0 and L, performing the standard separation of variables, and examining the behavior of each mode. The modes are sinusoids having wavelengths $W_n = 2L/n$; those modes for which $W_n > W_{CRIT}$ are oscillatory, though damped; those modes for which $W_n < W_{CRIT}$ are non-oscillatory, showing only the exponentially damped behavior. Note that this critical wavelength depends only on the tether properties, not on the length of the system. Another way of thinking of this critical length is that a freely hanging tether of length less than about L/2 (we have not actually done this calculation yet) should possess no oscillatory longitudinal modes. Attempts to include this internal damping (as opposed to external damping such as motion through a fluid) in the calculations for lateral ("plucked string") oscillations have resulted in a term coupling with the longitudinal oscillations. The effects of this term are not clear and are still under study.

We have two sources of information as to the damping in the tether material, both provided by Martin Marietta Corporation. These sources appear to differ substantially. First, there is a June 1983 report ("Analysis of Tethered Satellite Orbital Dynamics for Selected Mission Profiles, by Bodley and Park) which uses a value $C_V = 9.19 \times 10^4$ at one point in its analysis (p. 54); the source of this number is not clear, and it may be a preliminary value. Second, an internal report on "Tether Testing" dated September 1983 was kindly provided by A. C. Park of MMC; this report gives a "per cent damping" for an experimental setup consisting of a mass hanging on the end of a length of tether. We have calculated the damping coefficient from the experimental report

(but see the caveats below), and converted the earlier number to the same (mks) units. In summary:

- From the experimental data, AE $\approx 10^5$ kg-m/s^2 and $C_V \sim 200$ kg-m/s ("averaging" the experiments described). These imply a critically damped wavelength for tether longitudinal oscillations of about 25 meters (say, between 10 and 100).

- The value $C_V = 9.19 \times 10^4$ kg-km/hr given in the "... Orbital Dynamics ..." report, when converted to mks system becomes 2.6×10^4 kg-m/s. This is about 100 times greater than the value calculated from the experimental data above, and implies a critically damped wavelength of about 3 km. (The values for AE and μ, converted to mks, are consistent with the experimental AE and assumed 3 mm Kevlar at 1.5 g/cc density.)

Our interpretation of the experimental results, however, is somewhat uncertain since (1) the precise testing and computation procedures used were not clear, and (2) neither the direct experimental results nor a derived material property (C_V) were reported, but a "per cent damping", presumably the damping ratio for the experimental setup consisting of a 4.5 kg mass on the end of an 11 or 21 m "spring."

These calculations have been sent to A. C. Park at MMC for his comments and any light he may be able to shed on them. In any event, the implied critical damping scale, even of the smaller C_V value, is still significant for our studies and deserves further experimental determination.

2.3.3 High Resolution Loss-Of-Tension Model -

There has been no effort on this task in the present reporting period. Desirable extensions are the correct inclusion of damping (debugging a feature already coded), and the inclusion of gravity gradient force (which would retain the one-dimensional nature of the problem) and possibly Coriolis and drag, following the discussion of Section 2.3.1.3.

2.3.4 Analytical Studies Of The Slack Tether Problem -

There has been insufficient effort on this task in the present reporting period to report. Likely directions for continuing investigation include: transverse motions; tether constitutive relations, in particular determination of realistic constitutive relations for single-component and multi-component tethers from experimental data in hand; calculation of characteristic loop size for a "collapsing" tether after a break. This latter will have direct significance to tether safety issues.

2.3.5 Concluding Remarks -

The slack tether simulation program SLACK3 has been extended, made more easy to use, and made more resistant to failure. Several case studies have been simulated and analyzed. The relative effects of drag, Coriolis force, and the rebound of the tether after passing the Shuttle are beginning to become apparent. Cases in which SLACK3 has difficulty have been examined and found to stem primarily from physical situations where an actual tether would tend to come fully taut. These are intrinsically difficult for SLACK3 to handle with its current completely slack segment model. Future work with SLACK3 should

include minor debugging and running of cases of operational interest to NASA. Some effort may be given to modifying SLACK3 to operate at least sufficiently in taut cases, though a complete solution to this problem seems prohibitively difficult. An analytic study of the situations in which the cut tether fails to fully recoil past the Shuttle due to gravity gradient and other forces is underway and should clarify, or at least allow one to predict, those cases causing trouble to SLACK3.

The influence of tether properties, particularly the viscous damping C_v, on slack tether modeling has been examined. Experimental data appear to be preliminary, but those few available span the range in which the damping may seriously affect both the cut tether's physical behavior and our ability to model it. Definitive experiment is highly recommended.

Analytical studies are expected to progress in the next reporting period. Anticipated results are an estimate of the size of loops formed when the recoiling tether "buckles" in analogy with a column. The loop scale has obvious implications for tether safety studies. The high-resolution ball-and-spring model for tether breaks, which complements the analytic studies, may be enhanced to include damping and gravity gradient forces; out of line forces such as Coriolis, drag and bending stiffness might also be included.

2.4 Numerical Calculations Of The Electric Field Around An Electrodynamic Tether

2.4.1 General -

The evaluation of the potential hazards associated with the operation of an electrodynamic tether on board the Shuttle Orbiter requires a thorough modeling of the plasma environment in which the tether is embedded. As an initial step, we have embarked on an analytical effort under the simplifying assumption that the tether is deployed in vacuo. This initial effort will provide us with reference values against which we will compare the distribution of the electric field around the tether when plasma parameters will be introduced into the analysis.

In the first quarterly report we calculated the electric field at the tip of a 20 kilometer long wire, moving through the earth's magnetic field, modeled as a 40 kilometer long prolate spheroid in vacuo. The assumption was made that the spacecraft to which the other end of the wire is attached could be modeled as an infinite ground plane. It was shown in that report that the spheroidal model (which has a radius of curvature of 0.5 Å (5×10^{-9} cm) at its ends, therefore a dimension less than the diameter of an atom) is not a realistic representation of the electric field near the end of a physical wire. In fact, that model predicted an electric field of 1.145 teravolts/meter at a distance of 1 Å from the end of the wire and 4.5 teravolts/meter at the end of the wire. It was estimated in the first quarterly report that the electric field predicted by the spheroidal model was high by a factor of 2×10^{7}. This estimate was based on the assumption that the end of the wire was spherical and of the same diameter as the wire. To determine what the electric field would be, still in vacuo, at the end of a wire modeled as a uniform circular cylinder with a planar

end, we have started to adapt a program which was originally written to calculate magnetic scalar potential with a closed boundary to calculate electric field with an open boundary. The mesh on which the program iteratively solves Laplace's equation was replaced with one in which the mesh spacing varies geometrically. Thus in the neighborhood of the wire the axial lines are spaced 0.1 mm apart while at the outer edge of the mesh the spacing has increased to several meters.

Since the prolate spheroid is an excellent model of the far field of a thin wire, we have chosen to initialize the grid with potential values calculated by the spheroidal model.

2.4.2 Software Program Development -

To minimize the numerical problems encountered in the modeling of a long wire with an aspect ratio of 2×10^7 we tested the new program with a 400 meter long cylinder of 0.33 meter radius in vacuo. The grid on which the potentials are calculated extends axially from a point 44.25 meters beyond the end of the cylinder and radially from the axis of the cylinder to a distance of 40.15 meters from its axis. This distance resulted from the choice of a test grid 80 mesh boxes long and 40 mesh boxes in radius; with a mesh width of 10 cm at the end of the cylinder and a geometric factor of 1.1. Thus if the mesh box at the end of the cylinder is Δ_0 cm on each side, the mesh size n grid lines from the end will be $1.1^n \Delta_0$. Naturally only mesh boxes which lie on a diagonal line extending from the end of the cylinder at an angle of 45° to the axis will be square. A list of the axial and radial coordinates of the grid and the mesh box lengths and widths is given in Table 2.4.1.

CARD 2

IMAX	JMAX	NOBUG	ITMAX	ITMIN
40	80	1	1000	30

CARD 3

LINESF	DPID	ISPLC	NTEST
21	200.0000	5	5

	ZMETRIC	DELTAZ
1	159.8953	3.7404
2	163.6357	3.4004
3	167.0361	3.0913
4	170.0974	2.8102
5	172.9076	2.5548
6	175.4624	2.3225
7	177.7849	2.1114
8	179.8963	1.9194
9	181.8057	1.7449
10	183.5506	1.5863
11	185.1369	1.4421
12	186.5790	1.3110
13	187.8900	1.1918
14	189.0818	1.0835
15	190.1653	0.9850
16	191.1503	0.8954
17	192.0457	0.8140
18	192.8597	0.7400
19	193.5948	0.6728
20	194.2725	0.6116
21	194.8841	0.5560
22	195.4401	0.5054
23	195.9455	0.4595
24	196.4050	0.4177
25	196.8226	0.3797
26	197.2025	0.3452
27	197.5477	0.3138
28	197.8616	0.2853
29	198.1469	0.2594
30	198.4063	0.2358
31	198.6420	0.2144
32	198.8564	0.1949
33	199.0513	0.1772
34	199.2284	0.1611
35	199.3895	0.1464
36	199.5359	0.1331
37	199.6690	0.1210
38	199.7900	0.1100
39	199.9000	0.1000
40	200.0000	0.1000
41	200.1000	0.1100
42	200.2100	0.1210
43	200.3310	0.1331
44	200.4641	0.1464
45	200.6105	0.1611
46	200.7716	0.1772
47	200.9487	0.1949
48	201.1436	0.2144
49	201.3580	0.2358
50	201.5938	0.2594
51	201.8531	0.2853
52	202.1384	0.3138
53	202.4523	0.3452
54	202.7975	0.3797
55	203.1772	0.4177
56	203.5950	0.4595
57	204.0545	0.5054
58	204.5599	0.5560
59	205.1159	0.6116
60	205.7275	0.6728
61	206.4002	0.7400
62	207.1403	0.8140
63	207.9543	0.8954
64	208.8497	0.9850
65	209.8347	1.0835
66	210.9182	1.1918
67	212.1100	1.3110
68	213.4210	1.4421
69	214.8631	1.5863
70	216.4494	1.7449
71	218.1943	1.9194
72	220.1137	2.1114
73	222.2251	2.3225
74	224.5476	2.5548
75	227.1024	2.8102
76	229.9126	3.0913
77	[illegible]	3.4004
78	[illegible]	3.7404
79	[illegible]	4.1145
80	[illegible]	4.5259

	DELTAR
1	0.1000
2	0.1100
3	0.1210
4	0.1331
5	0.1464
6	0.1611
7	0.1772
8	0.1949
9	0.2144
10	0.2358
11	0.2594
12	0.2853
13	0.3138
14	0.3452
15	0.3797
16	0.4177
17	0.4595
18	0.5054
19	0.5560
20	0.6116
21	0.6728
22	0.7400
23	0.8140
24	0.8954
25	0.9850
26	1.0835
27	1.1918
28	1.3110
29	1.4421
30	1.5863
31	1.7449
32	1.9194
33	2.1114
34	2.3225
35	2.5548
36	2.8102
37	3.0913
38	3.4004
39	3.7404
40	4.1145

I= -199.99750
J1= 18.21237

FORMATS
ZMAX= 3.21965E+03 AT I= 40 J= 79
FORMAT (40I2/40I2)
ZMIN= 0.20339E+02 AT I= 4 J= 40
FORMAT (40I2/40I2)
FORMAT (I4,2X,72(0PF 8.2) /)

Table 2.4.1 Coordinates and mesh box dimensions for the grid.

2.4.3 Interpretation Of Plots Generated By The Code Laplace -

The grid was initialized with the spheroidal function on the assumption that the electric field in which the cylinder is immersed is otherwise uniform and of magnitude 1 volt/meter. The region occupied by the cylinder from mesh box 1 through mesh box 40 in the axial direction and from mesh box 1 through mesh box 3 in the radial direction is then set to zero to represent the zero potential cylinder. A plot of the electric equipotential surfaces around the end of the wire is shown in Figure 2.4.1. The grid which represents a region 84.404 meters long of radius 40.145 meters is actually 22.85 cm long. The two equipotential lines at the top are spaced 2 cm apart on the axis. Since the equipotential lines are spaced 10.98 volts apart this indicates an average axial electrical field E_z of 1.486 volt/meter. The calculated electric field for this region is shown in Table 2.4.2 from which we see an axial electric field of -1.43 volt/meter at position I=0, J=74. The electric fields printed in the figures are calculated at the center of the edges of the mesh boxes as shown in Figure 2.4.2.

The maximum electric field calculated for position I=3, J=39 is E_r = -620.33 V/m, E_z = 819.05 V/m. This value is not very accurate, because the potentials on the cylinder were set to zero while the potentials external to the cylinder were calculated in the absence of the cylinder. A more representative electric field is given at position I=0, J=40, when E_r = 0 V/m and E_z = -121.03 V/m.

Using the calculated potentials on the top and bottom edges of the grid, the outside radius and the surface of the cylinder as boundary conditions, the potential at all other points were calculated numerically using the Liebermann net procedure. A plot of the resulting electric field is shown in Figure 2.4.3. The axial electric field at position I=0, J=74 is shown in Table 2.4.3 as E_z = 1.55 V/m. The maximum electric field again occurs at position I=3, J=39, where

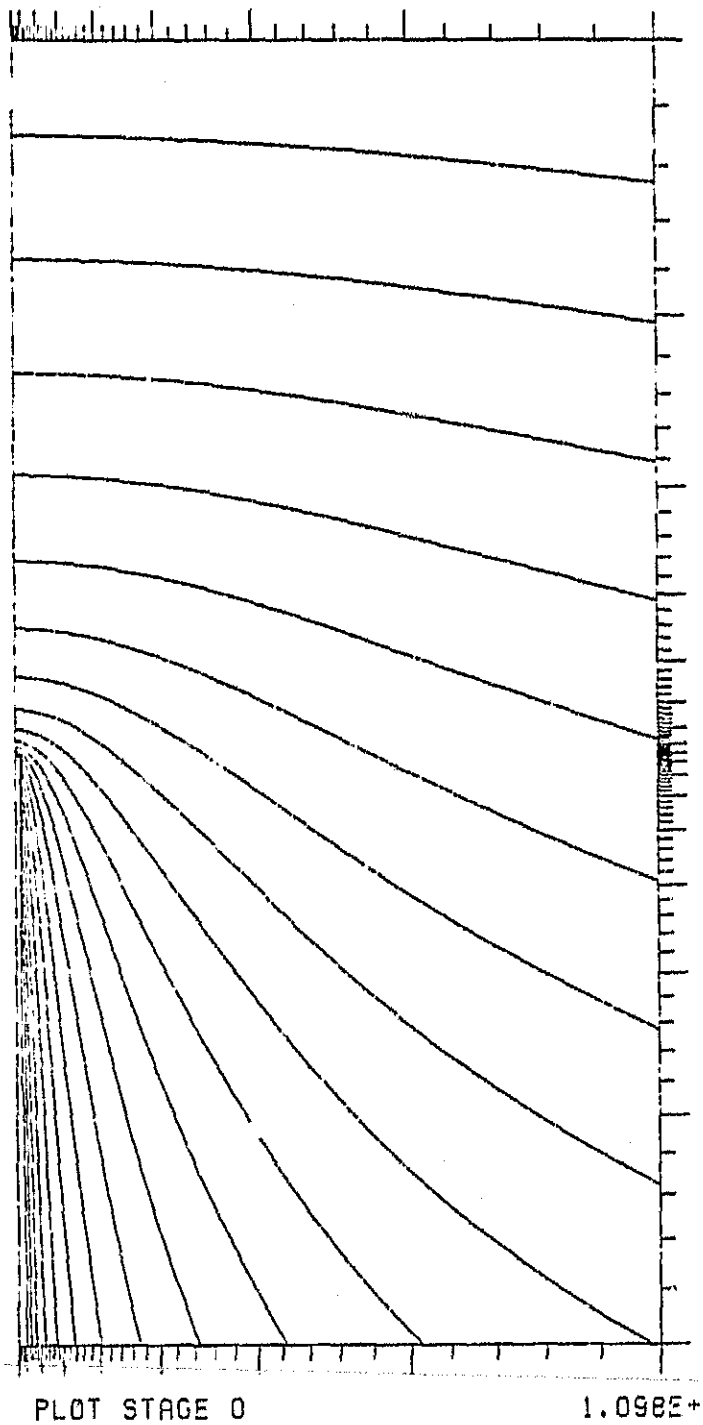

Figure 2.4.1 Analytical calculation of equipotential surfaces of the electric field around a prolate spheroid embedded in an otherwise uniform field.

I=	0	1	2	3	4	5	6	7	8	9	10	11	12	13	14
		VOLTMETER			FX.FOR TEST							<25-MAY-85>		<18:51:17>	
70	0.00	0.00	-0.01	-0.01	-0.02	-0.02	-0.02	-0.02	-0.03	-0.04	-0.05	-0.05	-0.06	-0.07	-0.08
	-1.71	-1.71	-1.71	-1.71	-1.71	-1.71	-1.71	-1.71	-1.71	-1.71	-1.71	-1.71	-1.71	-1.71	-1.70
71	0.00	0.00	-0.01	-0.01	-0.01	-0.02	-0.02	-0.02	-0.03	-0.03	-0.04	-0.04	-0.05	-0.06	-0.07
	-1.63	-1.63	-1.63	-1.63	-1.63	-1.63	-1.63	-1.63	-1.63	-1.63	-1.63	-1.63	-1.63	-1.63	-1.62
72	0.00	0.00	0.00	-0.01	-0.01	-0.01	-0.02	-0.02	-0.02	-0.03	-0.03	-0.04	-0.04	-0.05	-0.05
	-1.56	-1.56	-1.56	-1.56	-1.56	-1.56	-1.56	-1.56	-1.56	-1.56	-1.56	-1.56	-1.56	-1.55	-1.55
73	0.00	0.00	0.00	-0.01	-0.01	-0.01	-0.01	-0.02	-0.02	-0.02	-0.03	-0.03	-0.03	-0.04	-0.04
	-1.49	-1.49	-1.49	-1.49	-1.49	-1.49	-1.49	-1.49	-1.49	-1.49	-1.49	-1.49	-1.49	-1.49	-1.49
74	0.00	0.00	0.00	-0.01	-0.01	-0.01	-0.01	-0.01	-0.02	-0.02	-0.02	-0.02	-0.03	-0.03	-0.04
	-1.43	-1.43	-1.43	-1.43	-1.43	-1.43	-1.43	-1.43	-1.43	-1.43	-1.43	-1.43	-1.43	-1.43	-1.43
75	0.00	0.00	0.00	0.00	-0.01	-0.01	-0.01	-0.01	-0.01	-0.01	-0.02	-0.02	-0.02	-0.03	-0.03
	-1.38	-1.38	-1.38	-1.38	-1.38	-1.38	-1.38	-1.38	-1.38	-1.38	-1.38	-1.38	-1.38	-1.38	-1.38
76	0.00	0.00	0.00	0.00	0.00	-0.01	-0.01	-0.01	-0.01	-0.01	-0.01	-0.02	-0.02	-0.02	-0.03
	-1.34	-1.34	-1.34	-1.34	-1.34	-1.34	-1.34	-1.34	-1.34	-1.34	-1.34	-1.34	-1.34	-1.34	-1.34
77	0.00	0.00	0.00	0.00	0.00	0.00	-0.01	-0.01	-0.01	-0.01	-0.01	-0.01	-0.02	-0.02	-0.02
	-1.30	-1.30	-1.30	-1.30	-1.30	-1.30	-1.30	-1.30	-1.30	-1.30	-1.30	-1.30	-1.29	-1.29	-1.29
78	0.00	0.00	0.00	0.00	0.00	0.00	0.00	-0.01	-0.01	-0.01	-0.01	-0.01	-0.01	-0.01	-0.02
	-1.25	-1.25	-1.26	-1.26	-1.26	-1.26	-1.26	-1.26	-1.26	-1.26	-1.26	-1.25	-1.26	-1.26	-1.26
79	0.00	0.00	0.00	0.00	0.00	0.00	0.00	-0.01	-0.01	-0.01	-0.01	-0.01	-0.01	-0.01	-0.01
	-1.23	-1.23	-1.23	-1.23	-1.23	-1.23	-1.23	-1.23	-1.23	-1.23	-1.23	-1.23	-1.23	-1.23	-1.23

Table 2.4.2 Values of electric field computed on the basis of analytically calculated potentials.

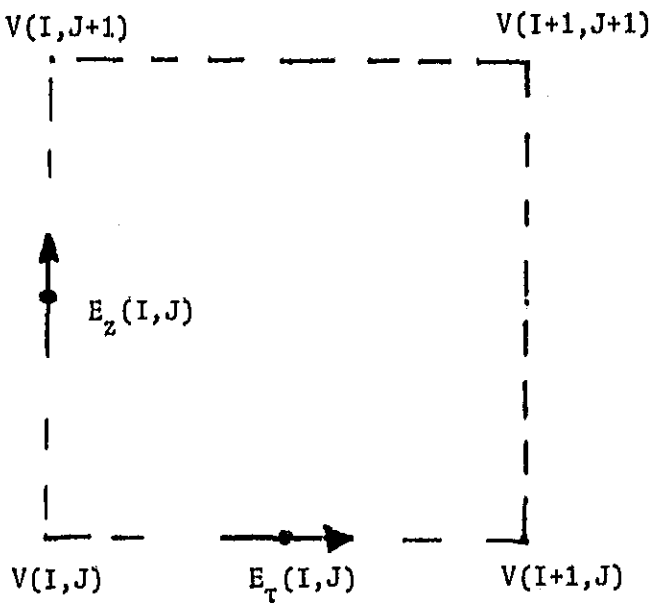

Figure 2.4.2 This diagram shows the position at which E_r and E_z are calculated for each mesh box. The naming convention adopted is that each electric field is labeled by the coordinates (I,J) of the lower left hand corner of the mesh box.

E_r = -235.69 V/m and E_z = -187.03 V/m. This result is correct because the zero cylinder potential was one of the boundary conditions for the numerical calculation. The axial field at I=0, J=40 is shown to be -115.76 V/m and at I=0, J=39 as E_z = -124.35 V/m.

The plots and tables of electric field shown here were calculated to test the new software program in a relatively easy case. When a wire modeled as a cylinder 4000 m long and 2 mm diameter was calculated, we found that roundoff error caused numerical instability in the analytic functions used to initialize the grid. These functions are correctly calculated in double precision on a Control Data computer (29 places) but the shorter word length of the VAX does not permit their use. We are testing approximation techniques to calculate the function

$$\log\left(\frac{\xi+1}{\xi-1}\right)$$

in the limit as ξ approaches 1.

This modification of the software program (which is not yet complete at the time of this writing) will be illustrated in the next quarterly report.

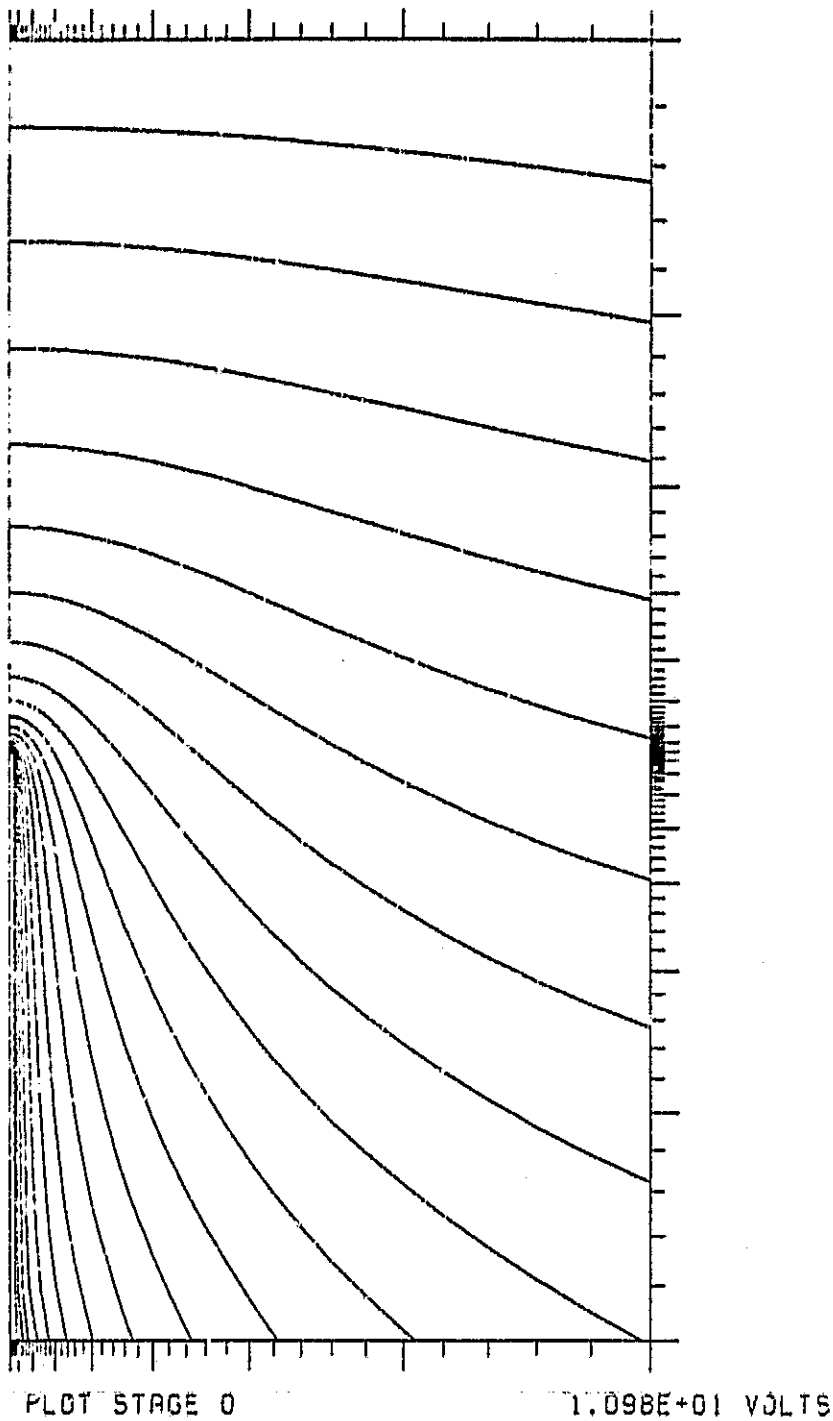

Figure 2.4.3 Numerical computation of equipotential surfaces as in Figure 2.4.1.

	2	1	2	3	4	5	6	7	8	9	10	11	12	13	14
10	-0.01 -1.59	0.00 -1.56	-0.01 -1.56	-0.02 -1.62	-0.03 -1.56	-0.04 -1.50	-0.06 -1.56	-0.07 -1.56	-0.09 -1.89	-0.10 -1.89	-0.11 -1.89	-0.13 -1.89	-0.15 -1.88	-0.17 -1.88	-0.19 -1.87
11	0.00 -1.79	0.00 -1.79	-0.01 -1.79	-0.01 -1.79	-0.02 -1.79	-0.03 -1.79	-0.04 -1.79	-0.05 -1.79	-0.06 -1.79	-0.08 -1.79	-0.09 -1.79	-0.10 -1.79	-0.12 -1.78	-0.13 -1.78	-0.15 -1.78
12	0.00 -1.70	0.00 -1.70	-0.01 -1.70	-0.01 -1.70	-0.02 -1.70	-0.03 -1.70	-0.04 -1.70	-0.04 -1.70	-0.05 -1.70	-0.06 -1.70	-0.07 -1.70	-0.08 -1.70	-0.09 -1.70	-0.11 -1.69	-0.12 -1.69
13	0.00 -1.62	0.01 -1.62	0.00 -1.62	-0.01 -1.62	-0.02 -1.62	-0.02 -1.62	-0.03 -1.62	-0.04 -1.62	-0.04 -1.62	-0.05 -1.62	-0.06 -1.62	-0.07 -1.62	-0.08 -1.62	-0.09 -1.62	-0.10 -1.61
14	0.00 -1.55	0.00 -1.55	0.00 -1.55	-0.01 -1.55	-0.01 -1.55	-0.02 -1.55	-0.03 -1.55	-0.03 -1.55	-0.04 -1.55	-0.04 -1.55	-0.05 -1.55	-0.05 -1.55	-0.06 -1.55	-0.07 -1.55	-0.08 -1.55
15	0.00 -1.50	0.00 -1.50	-0.01 -1.50	-0.01 -1.50	-0.02 -1.50	-0.02 -1.50	-0.02 -1.49	-0.03 -1.49	-0.03 -1.49	-0.03 -1.49	-0.04 -1.49	-0.04 -1.49	-0.05 -1.49	-0.06 -1.49	-0.06 -1.49
16	0.00 -1.44	-0.01 -1.44	-0.01 -1.44	-0.01 -1.44	-0.01 -1.44	-0.01 -1.44	-0.02 -1.44	-0.02 -1.44	-0.03 -1.44	-0.03 -1.44	-0.03 -1.44	-0.04 -1.44	-0.04 -1.44	-0.04 -1.44	-0.05 -1.44
17	0.00 -1.40	0.00 -1.40	0.00 -1.40	-0.01 -1.40	-0.01 -1.40	-0.01 -1.40	-0.01 -1.40	-0.02 -1.40	-0.02 -1.40	-0.02 -1.40	-0.02 -1.40	-0.03 -1.40	-0.03 -1.40	-0.03 -1.40	-0.04 -1.40
18	0.00 -1.37	0.00 -1.37	0.00 -1.37	0.00 -1.37	-0.01 -1.37	-0.01 -1.37	-0.01 -1.37	-0.01 -1.37	-0.01 -1.37	-0.02 -1.36	-0.02 -1.36	-0.02 -1.36	-0.02 -1.36	-0.03 -1.36	-0.03 -1.36
19	0.00 -1.34	0.00 -1.34	0.00 -1.34	0.00 -1.34	0.00 -1.34	0.00 -1.34	-0.01 -1.34	-0.01 -1.34	-0.01 -1.34	-0.01 -1.34	-0.01 -1.34	-0.01 -1.34	-0.02 -1.34	-0.02 -1.34	-0.02 -1.34

Table 2.4.3 Values of electric field computed on the basis of numerically calculated potentials.

3.0 PROBLEMS ENCOUNTERED DURING REPORTING PERIOD

Significant progress has been made in the development of the three-dimensional electrodynamic computer code for the evaluation of the electric potential around a severed tether in vacuo. Numerical results for a test case tether severance with a short tether length are presented in this quarterly report. Longer tethers are still difficult to deal with because of numerical accuracy problems. These problems have impeded us to show plots of the electric field around a severed tether of substantial tether length. However, a solution to this problem has been singled out and computations for longer tethers will be performed during the next reporting period.

4.0 ACTIVITY PLANNED FOR THE NEXT REPORTING PERIOD

The study of retrieval control algorithms will be continued with some study of the stability of simple rate control laws. The study of thruster control algorithms will be continued with possible topics including control of out-of-plane librations, yaw control, use of the in-line thruster, and the effect of rigid body rotations of the subsatellite.

Future work with SLACK3 will include minor debugging and running of cases of operational interest to NASA. The capability to accelerate the Shuttle in order to avoid the recoiling tether will be implemented in the computer code and cases will be run. Analytical studies on tether detensioning are expected to progress in the next reporting period. Anticipated results are an estimate of the size of the loops when the recoiling tether "buckles" in analogy with a column.

The computer code for electric field computations will be improved. The electric field around tethers in vacuo severed far from the Shuttle will be computed. Modification of this computer code to include plasma characteristics appears to be much more complicated than expected. During the next reporting period simplified computations with the plasma will be attempted to have indications on the potentially hazardous situations.